Numerical simulation of bacterial flora in the intestine of zebrafish larvae

Numerical simulation of bacterial flora in the intestine of zebrafish larvae (ゼブラフィッシュ稚魚の腸内フローラの数値シミュレーション)

Jinyou Yang

January 29, 2019

Tohoku University
Graduate School of Biomedical Engineering
Department of Biomedical Engineering

指導教員	石川　拓司　教授
審　査　委　員 （○印は主査）	○ 石川　拓司　教授 1　福島　浩平　教授　　2　太田　信教授 3　菊地　謙次　准教授

、

Abstract

Zebrafish has been used in scientific research as organism model, due to its many advantageous factors, such as the transparency of zebrafish larvae. Many researchers use it in studies of gastrointestinal diseases and the microbial flora of the gut. Although many researches about the intestine of zebrafish larvae have been conducted, the transport phenomena and the bacterial spatial distribution in the intestine of zebrafish larvae have not been fully clarified.

In chapter 1 of this thesis, we reviewed the advantageous factors of zebrafish and the related researches about intestine and gut flora of zebrafish larvae. The anatomy of zebrafish larval intestine, the zebrafish model for disease, the microbial flora spatial distribution in the zebrafish intestine, and the objective of this thesis were introduced in this chapter.

In chapter 2 of this thesis, transport caused by peristaltic motion in the intestine of zebrafish larvae was investigated first by numerical simulation. An anatomically realistic three-dimensional geometric model of the intestine at various times after feeding was constructed based on the experimental data of Field et al. (2009). The flow of digested chyme was analyzed using the governing equations of fluid mechanics, together with peristaltic motion and long-term contraction of the intestinal wall. The results showed that retrograde peristaltic motion was the main contributor to the mixing function. The dispersion caused by peristalsis over 30 min was in the order of 10^{-12} m^2/s, which is greater than the Brownian diffusion of a sphere of 0.4 μm diameter. In contrast, anterograde peristaltic motion contributed mainly to the pumping function. The pressure decrease due to peristalsis was in the order of millipascals, which may reduce the activation and maintenance heat of intestinal muscle.

In chapter 3 of this thesis, the bacterial spatial distribution in the intestine of zebrafish larvae was investigated, because microbial flora in the intestine has been thoroughly validated that it plays an important role in the health of the host. Jemielita et al. (2014) showed experimentally that Aeromonas bacteria in the intestine of zebrafish larvae have a heterogeneous spatial distribution. Although bacterial aggregation is important biologically and clinically, there is no mathematical model describing the phenomenon and its mechanism remains largely unknown. We thus developed a computational model to describe the heterogeneous distribution of bacteria in the intestine of zebrafish larvae. The results showed that biological taxis could cause the bacterial aggregation. Intestinal peristalsis had the effect of reducing bacterial aggregation through mixing function. Using a scaling argument, we showed that the taxis velocity of bacteria must be larger than the sum of the diffusive velocity and background bulk flow velocity to induce bacterial aggregation.

In chapter 4 of this thesis, based from the results of this thesis, we concluded our findings in this thesis will be useful for a greater understanding of the mixing and pumping functions of the intestine of zebrafish larvae. Our computational model of bacteria aggregation will be useful to further the scientific understanding of intestinal microbial flora.

Table of Contents

List of Figures

Chapter 1

Introduction

1.1 Zerbrafish

The zebrafish, *Danio rerio*, has emerged as a major model organism for biomedical research during the last decade, due to its many advantageous factors[5, 8, 14, 17, 26, 34]. For example, the zebrafish is small and robust, which is cheaper to maintain than mice. Zebrafish biology allows ready access to all developmental stages. The optical clarity of embryos and larvae allow researchers to easily examine the development of internal structures and real-time imaging of developing pathologies. Due to the nearly transparent(seen Figure1.1), the blood vessel in a living zebrafish embryo can be seen using just a low-power microscope[5, 34, 38]. Hundreds of zebrafish offspring at weekly intervals can provide scientists with an ample supply of embryos to study[73]. And they grow at an extremely fast rate, developing as much in a day as a human embryo develops in one month. Zebrafish have a similar genetic structure to humans. Many of the zebrafish mutant phenotypes identified ingenetic screens are reminiscent of human disease states, providing a powerful approach for gaining insight to the corresponding pathophysiology[14, 16]. The zebrafish genome has been fully sequenced to a very high quality. This has enabled scientists to create mutations to study their function[30, 53, 63]. As a vertebrate, zebrafish organs are functionally and morphologically similar to the human, their muscle, blood, kidney and eyes share many features with human systems. So it was hoped that the screens additionally might unveil mechanisms and pathways directly relevant to human disease and therapy.

Zebrafish has been used as a model organism to study the human disease for

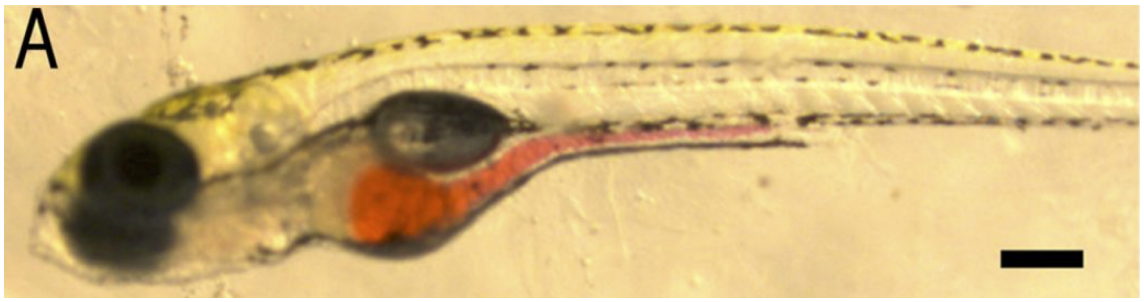

Figure 1.1. Image of a larval zebrafish at 5 days post-fertilization. Scale bar, 250 µm (adapted from [29])

many aspects. Egan et al.[17] used zebrafish as model organism for experimental studies of stress and anxiety, and confirmed zebrafish as a valid, reliable, and high-throughput model of stress and affective disorders. Zebrafish have the unique ability to repair heart muscle[5, 35]. For example, if part of their heart is removed they can grow it back in a matter of weeks. Scientists are working to find out the specific factors involved in this process to see if this will help us to develop ways of repairing the heart in humans with heart failure or who have suffered heart attacks[45, 53, 61]. Zon et al.[73] reported that by combining the scale and throughput of in vitro screens with the physiological complexity of animal studies, the zebrafish promises to contribute to several aspects of the drug development process, including target identification, disease modelling, lead discovery and toxicology. Jordan et al.[61] reviewed that the modular medical models of zebrafish for human from the heart, vascular disease, kidney, skeleton, blood, brain, behavior, ear, eye, to the gastrointestinal gut.

The zebrafish intestine microanatomically resembles the human intestine in many regards. The red part in Figure 1.1 is the intestine of a zebrafish larve. An epithelial layer lines the lumen, with cell division in the intervillus spaces providing a renewing population for sloughed epithelium. There is no stomach in the zebrafish, but there are regions that predominantly participate in the digestion of proteins, fat, and ions, mimicking the anatomic divisions in humans. Intestinal motility in the zebrafish results from contractions of an inner circular and outer longitudinal layer of smooth muscle. Peristalsis begins by 4 dpf and becomes coordinated one day later. So many researchers studied digestive physiology in vivo in the zebrafish [2, 5, 29, 49, 61].

1.2 Gut microbiota

Gut microbiota is found in virtually any metazoan, from invertebrates to vertebrates. It has long been believed that gut microbiota, more specifically, the activity of the microbiome and its metabolic products, directly influence a variety of aspects in metazoan physiology[37, 59]. The composition and activity of the gut microbiota codevelop with the host from birth. An internal body cavity surrounding the gut and other organs and have coevolved with a diverse range of symbiotic gut bacteria and other microorganisms collectively known as the gut microbiota. For huamns, a complex gastro-intestinal microbiota that includes all three domains of life (Archaea, Bacteria and Eukarya) is harboured, and this characteristic and complex mixtures of microorganisms that have coevolved with their human hosts[12, 13]. The role of these gut microbial communities in our evolution is a matter of considerable interest.

The gut microbiota is essential for the development and function of the mucosal immune system during early life, a process that is now known to be important to overall immunity in adults. An absence of intestinal bacteria is associated with reductions in mucosal cell turnover, vascularity, muscle wall thickness, motility, baseline cytokine production, and digestive enzyme activity and with defective cell-mediated immunity. Furthermore, the intestinal microflora makes important metabolic contributions to vitamin K, folate, and short-chain fatty acids, such as butyrate, a major energy source for enterocytes, and also mediates the break-down of dietary carcinogens[6, 7, 44].

In humans, the shaping of these gut microbiota is then driven by a series of complex and dynamic interactions throughout life, including diet, life-style, disease, and antibiotic use[44]. In the healthy state, these gut microbiota contribute nutrients and energy to the host via the fermentation of nondigestible dietary components in the large intestine, and a balance is maintained with the host's metabolism and immune system. Negative consequences, however, can include acting as sources of inflammation and infection, involvement in gastrointestinal diseases, and possible contributions to diabetes mellitus and obesity[7, 22, 46, 59]. The bacterial flora of the gastrointestinal tract varies longitudinally; the oral cavity contains about 200 different species, the stomach is almost sterile, and the bacterial content increases distally, with approximately 10^8 bacteria per g (dry weight) of ileal contents and up to 10^{12} bacteria per g (dry weight) of colonic contents[6, 7].

The understanding of principles governing the localization of intestinal bacteria, and spatial relationships between bacteria and their hosts is very important[65, 66]. Variation in microbial localization and density within the digestive tract has been described along both the length of the gut (from mouth to rectum) and the cross-section (from mucosa-associated into the lumen). The vast majority of gut bacteria are found within the transient digesta passing through the lumen of the lower gastrointestinal tract. In the small intestine, where transit is faster, and simple sugar and amino acid metabolism is favored, the community is dominated by rapidly dividing facultative anaerobes such as *Proteobacteria* and *Lactobacillales*. By contrast, in the large intestine the flow is slower, and metabolism favors fermentation of complex polysaccharides derived either from undigested plant material or from the host mucus. Within the colon, bacteria are also organized along the transverse axis, from the middle of the lumen to the mucosa. Moving toward the epithelium, mucin utilizers, such as *Akkermansia muciniphila* are thought to be enriched[11]. Historically, research into the impact of the microbiota on human health has focused on either compositional changes associated with disease, or the emergence of pathogens that can colonize or breach the epithelium. Now, it is becoming clear that spatial reprogramming of the microbiota may be a common and functionally relevant feature of chronic inflammatory diseases [65].

1.3 Former studies

Due to the advantage of the zebrafish, many research about intestine and gut flora in the intestine of zebrafish were developed. The development and anatomy of the zebrafish digestive system had been investigated in detail[10, 19, 20, 42, 43, 67]. Between 26 and 126 hours post-fertilization (hpf) of the zebrafish, the lumen formation and differentiation of a continuous layer of endoderm into a functional intestinal epithelium with three morphologically distinct segments: the intestinal bulb, mid-intestine and posterior intestine. Spontaneous regular gut motility in zebrafish begins around 4 days post fertilization (dpf) and comprises anterograde and retrograde peristalsis[24](seen Figure1.2). Roach et al.[54] investigated the frequency, travel distance and travel velocity of peristaltic motion and found that the frequency of anterograde peristalsis was greater than that of retrograde peristalsis. Holmberg et al.[23, 24] used tetrodotoxin to elucidate the role of nervous control in antero-

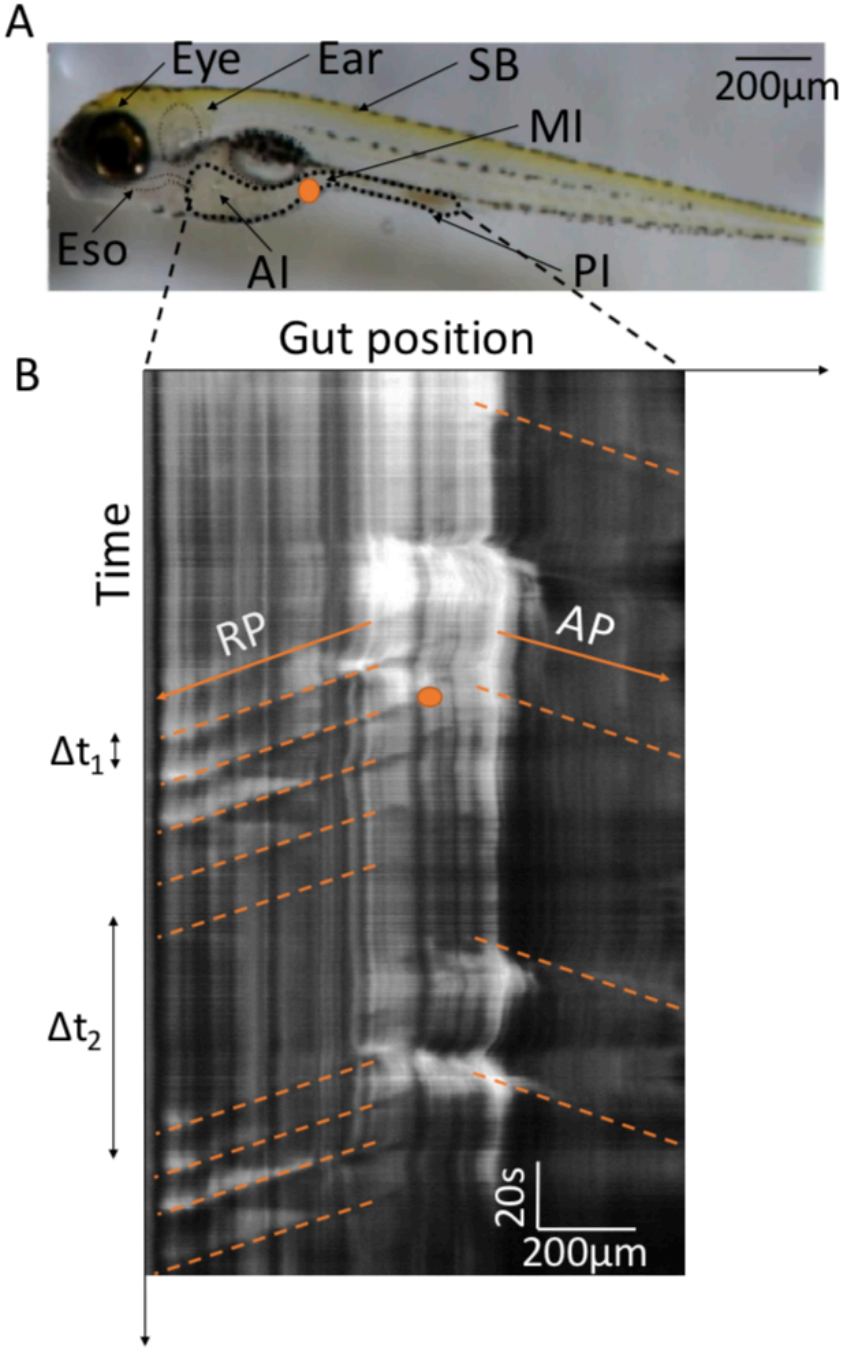

Figure 1.2. Visualization of the intestine peristalsis of the zebrafish larva at 7 dpf (days post fertilization), 6 hours post-inoculation with the rhodamine B solution (2mM). (A) Organ structure of zebrafish larva at 7 dpf. SB = swim bladder, Eso = esophagus, AI = anterior intestine, MI = middle intestine, PI = posterior intestine. (B) Time history of propagating peristaltic motion with the retrograde and anterograde peristalses. RP = retrograde peristalsis, AP = anterograde peristalsis(Ref. Graduation thesis of Noh Hyeong Tak (2016)).

grade and retrograde peristaltic motion in the intestine of zebrafish larvae. Their results showed that anterograde and retrograde peristaltic motions originated from the same region, and nerves played an important role as modulators of intestinal activity. Transport phenomena in the zebrafish intestine were investigated by Field et al.[18], who non-invasively monitored the passage of luminal contents through the intestine for 24 h and assessed the physiological consequences of the absence or reduced numbers of enteric neurons. Cocchiaro and Rawls[8] also non-invasively monitored the passage of luminal contents through the intestine for 24 h and discussed intestinal motility. The transport phenomena in the zebrafish intestine is very important, but have not been fully clarified. In particular, the peristaltic functions of the zebrafish intestine are unclear.

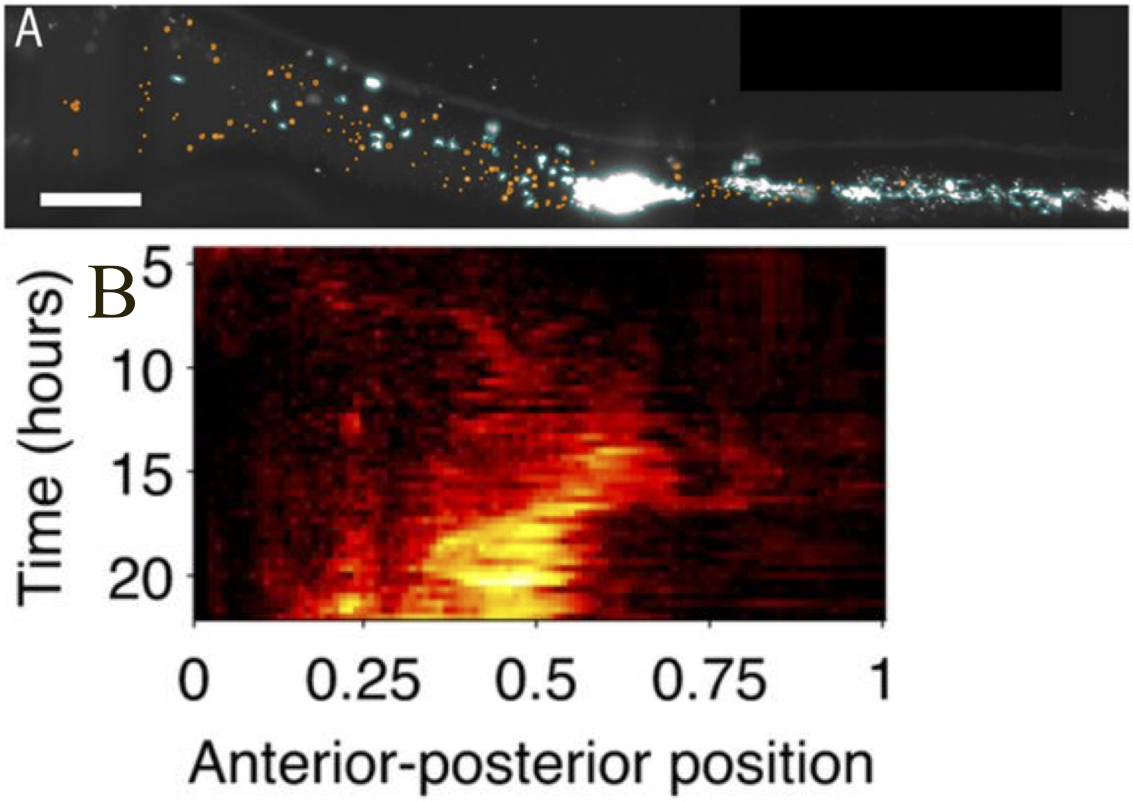

Figure 1.3. (A)Maximum intensity projection at 15.6 h post-inoculation with dTomato-labeled A. veronii. Scale bar, 100 µm.(B) Heat map showing the averaged anterior-posterior location in the zebrafish intestine of clusters of *A.veronii* with zero being the beginning of the intestine and 1 being the end of host autofluorescent intestinal cells, excluding bacteria located by the vent.(adapted from [29]).

Bacteria in the intestine play important role in the hosts' normal development and health[3]. Hecne, many researchers used the zebrafish as a model to do the studies on the bacterial flora in the intestine of zebrafish[2, 29, 49, 55, 71]. Bates et al.[3] found that in the absence of the microbiota, the gut epithelium was arrested in aspects of its differentiation, as revealed by the lack of brush border intestinal alkaline phosphatase activity, the maintenance of immature patterns of glycan expression and a paucity of goblet and enteroendocrine cells. Rolig et al.[55] concluded that the proportional representation of bacteria in a community does not necessarily predict its functional capacities; however, characterizing specific properties of individual species offers predictive insights into multispecies community function. Vander Sar et al.[58] used the 28 h-old zebrafish embryos to determine the exact location and fate of these bacterial pathogens in a livingvertebrate host. Rendueles et al.[51] developed a zebrafish model of controlled co-infection in which germ-free zebrafish raised on axenic living protozoa enabled the study of interactions between host and commensal and pathogenic bacteria. The bacterial composition along the intestinal tract of zebrafish was investigated by Lan et al.[33] with cultivation-independent analysis of the 16S rRNA gene. Jemielita et al.[29] reported that *Aeromonas* bacteria in the larval zebrafish intestine exhibit a heterogeneous distribution and are aggregated in the middle of the intestinal tract(seen Figure1.3). Wiles et al.[71] further investigated the distribution of *Aeromonas* by introducing another bacterium, $Vibrio$, into the larval zebrafish intestine. They showed that the habitat of *Aeromonas* was modified by competition with $Vibrio$, resulting in altered distribution. Although the distribution of bacteria in the intestine is very important biologically and clinically, its mechanism is not fully clarified.

1.4 Objective

With the background described in the previous sections, the mechanism of transport and bacterial aggregation phenomena in the intestine of zebrafish larvae are not clearly clarified. Hence, the objectives of this thesis are summarized as follows:

1. To perform a numerical simulation of the transport phenomena in the intestine of a zebrafish larvae and then to demonstrate this transport phenomena. In particular, to clarify the mixing and pumping functions of the zebrafish intestine (Chapter 2),

2. To introduce a computational model to describe the heterogeneous distribution of bacteria in the intestines of zebrafish larvae (Chapter 3).

Chapter 2

Transport caused by peristaltic motion in the zebrafish intestine

2.1 Introduction

The zebrafish has a genetic structure and major organs similar to those of humans. Zebrafish larvae are almost transparent, which facilitates monitoring the development of internal structures. Therefore, zebrafish have been widely used in studies of vertebrate biology as a model organism [4, 38–41, 70]. The development and anatomy of the zebrafish digestive system were investigated by Wallace et al.[67, 68]. Shin and Fishman [61] showed that human diseases of the gastrointestinal tract—such as colorectal cancer, dysmotility and malabsorption—resembled those in zebrafish. The microbial flora of the zebrafish intestine plays key roles in the development and health of the host. The spatial and temporal dynamics of the microbial flora of the zebrafish intestine were investigated by Bates et al.[3] and Jemielita et al.[29]. Rawls et al.[50] non-invasively observed bacterial motility and symbiosis in the zebrafish intestine. Bacterial growth is influenced by mass transport in the intestine, which is dominated by momentum transport, *i.e.*, flow. Therefore, for comprehensive understanding of the microbial flora of the intestine, the transport phenomena therein must be investigated.

The anatomy and histology of the zebrafish intestine have been reported [42, 67]. The peristaltic motion of the zebrafish intestine, which comprises anterograde and retrograde peristalsis, has also been the subject of research. Roach et al[54]. investigated the frequency, travel distance and travel velocity of peristaltic motion and found that the frequency of anterograde peristalsis was greater than that of

retrograde peristalsis. Holmberg[23, 24] used tetrodotoxin to elucidate the role of nervous control in anterograde and retrograde peristaltic motion in the intestine of zebrafish larvae. Their results showed that anterograde and retrograde peristaltic motions originated from the same region, and nerves played an important role as modulators of intestinal activity. Transport phenomena in the zebrafish intestine were investigated by Field et al.[18], who non-invasively monitored the passage of luminal contents through the intestine for 24 h and assessed the physiological consequences of the absence or reduced numbers of enteric neurons. Cocchiaro and Rawls[8] also non-invasively monitored the passage of luminal contents through the intestine for 24 h and discussed intestinal motility. However, the transport phenomena in the zebrafish intestine have not been fully clarified. In particular, the mixing and pumping functions of the zebrafish intestine are unclear. To address these issues, a numerical simulation of the transport phenomena in the larval zebrafish intestine was performed. An anatomically realistic three-dimensional geometric model of the intestine at various times after feeding was constructed based on the experimental data of Field et al.[18]. The flow of digested chyme was analyzed using the governing equations of fluid mechanics, together with peristaltic motion and long-term contraction of the intestinal wall. The results showed that retrograde peristaltic motion contributed mainly to the mixing function, whereas anterograde peristaltic motion contributed to the pumping function.

2.2 Modeling and Methods

2.2.1 Geometry of the intestine

The geometry of the intestine of a zebrafish larva at 7 days was obtained from images in Field et al.[18]. using the image analysis software ImageJ(NIH, USA). The origin of coordinates was set at the inlet of the intestine, *i.e.*, just past the esophageal sphincter, and the z-axis was defined so as to encompass the cross-sectional center of the outlet. The width of the intestine as a function of z was calculated using ImageJ, and the centerline of the intestine was extracted. The cross section of the intestine was assumed to be circular based on a previous report that the intestine of zebrafish larvae at 7 days has an approximately circular cross section [1, 3, 54]. The three-dimensional geometry of the intestine was then constructed based on the

centerline and diameter. Field et al.[18] reported the geometry of the intestine of zebrafish larvae for 24 h after feeding. Initially, the anterior part of the intestine expands due to feeding and then contracts gradually. To express this contraction of the intestine, the following equations were used:

$$W_l(z,t) = W_{24}(z) + g(z,t), \tag{2.2.1}$$

$$g(z,t) = \delta_g exp\left(\frac{-t}{\tau_g}\right) exp\left\{\frac{ln0.5}{\lambda_g^2}(z - z_{g0})^2\right\}, \tag{2.2.2}$$

where $W_l(z,t)$ is the diameter of the intestine without short-term peristaltic motion but with long-term contraction $g(z,t)$. In Eq.(2.2.2), δ_g indicates the amplitude of the expansion, τ_g is the relaxation time of the contraction, λ_g is the half-width of the expansion, and z_{g0} is the position of the expansion. In Eq.(2.2.1), $W_{24}(z)$ is the diameter of the intestine 24 h after feeding, *i.e.*, the final shape. The geometry of the intestine at t = 24 h is shown in Figure2.1. The fitting parameters in Eq.(2.2.2) are provided in Table 2.1. Comparisons between Eq.(2.2.2) and the findings of Field et al.[18] are shown in Figure2.2.

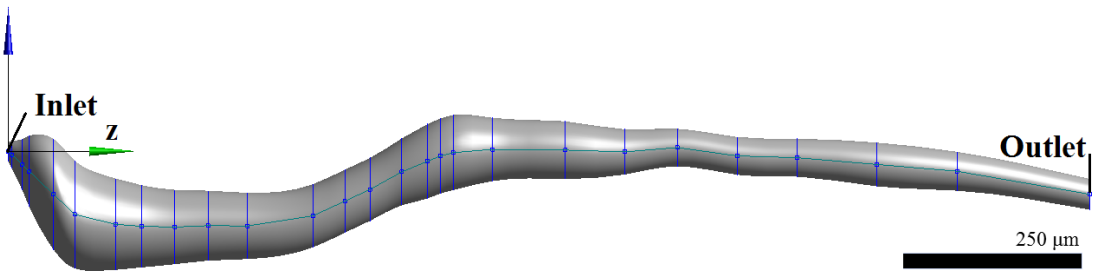

Figure 2.1. A three-dimensional model of the intestine of a zebrafish larva at 7 days (t = 24 h).

In addition to long-term contraction, two major types of short-term peristaltic motion are generated in the zebrafish intestine. Retrograde peristalsis propagates towards the inlet, whereas anterograde peristalsis propagates towards the outlet. Both peristaltic waves originate immediately distal to the end of the swim bladder z_{f0} [24, 54]. By superimposing the two types of short-term peristaltic motion, given by $f(z,t)$in a manner similar to that of Ishikawa et al.[28], the diameter of the intestine with short-term peristalsis and long-term contraction, $W(z, h+t)$, is given

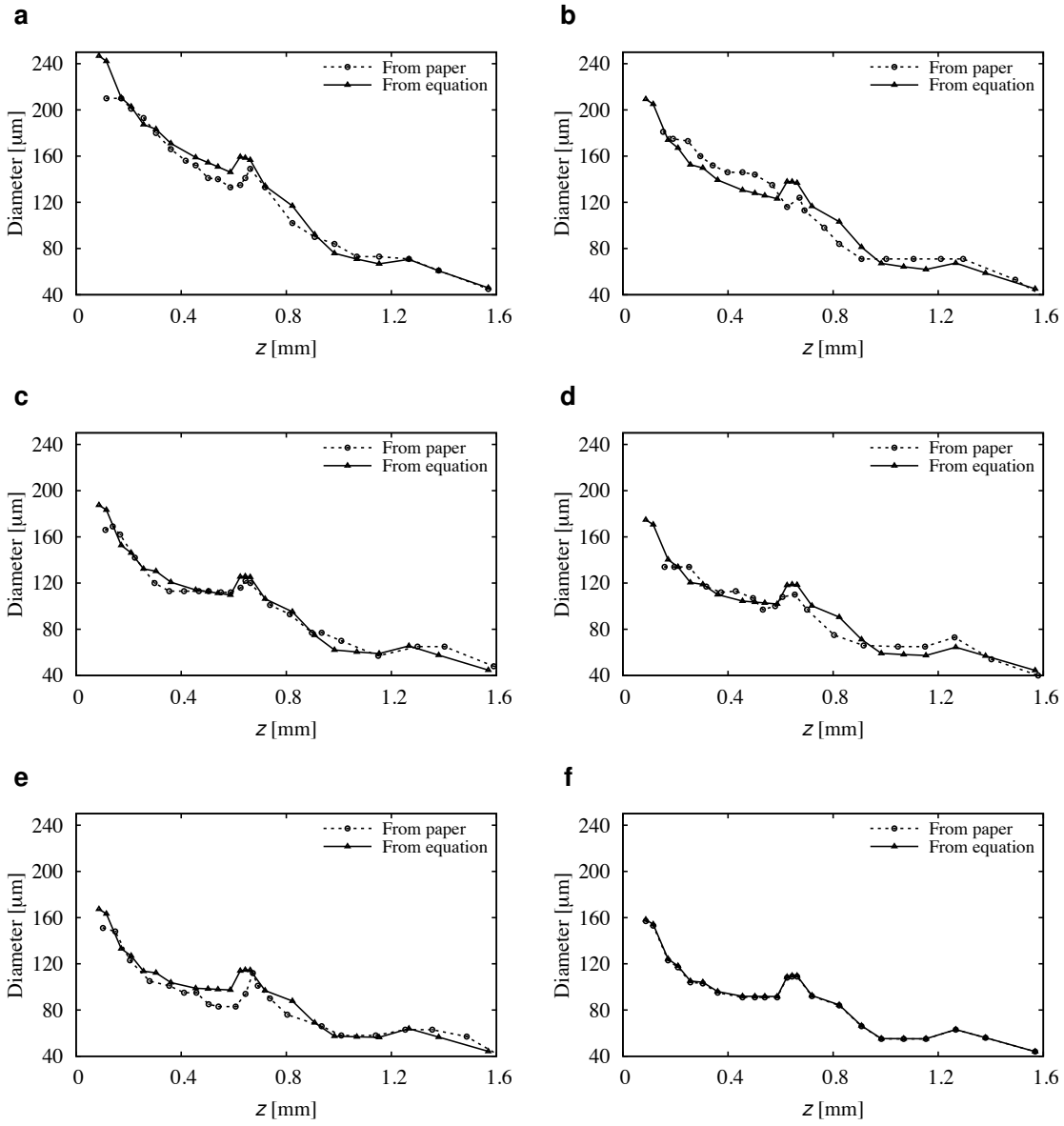

Figure 2.2. Comparison of the intestinal geometries of the model given by Eq.2.2.1 and those reported by Field et al.[18]: (a) $h = 0$ h, (b) $h = 3$ h, (c) $h = 6$ h, (d) $h = 9$ h, (e) $h = 12$ h, and (f) $h = 24$ h

as:

$$W(z, h+t) = W_l(z, h) + f_{an}(z, t) + f_{re}(z, t) + ct\frac{\partial g(z,t)}{\partial t}|_{(t=h)}, \tag{2.2.3}$$

$$f_{an}(z, t) = -\delta_f J(z, d_{an}) exp\left[\frac{ln0.5}{\lambda_f^2}\{z - H(t, \Delta t_{an})U_c - z_{f0}\}^2\right], \tag{2.2.4}$$

$$f_{re}(z, t) = -\delta_f J(z, d_{re}) exp\left[\frac{ln0.5}{\lambda_f^2}\{z - H(t, \Delta t_{re})U_c - z_{f0}\}^2\right], \tag{2.2.5}$$

where h was set as 0, 3, 6, 12 or 24 h in this study, and the time course after h was investigated. The functions $f_{an}(z, t)$ and $f_{re}(z, t)$ are anterograde and retrograde peristaltic motion, respectively. In each function, δ_f is the depth of the peristaltic waveform, λ_f is the half-width, and U_c is the wave propagation velocity. The function $J(z, d)$ was used to express the gradual disappearance of short-time peristalsis, and it is defined as:

$$J(z, d) = \begin{cases} 1, & when\ |z - z_{f0}| \leq d \\ exp[-\dfrac{(|z - z_{f0}| - d)}{l}], & when\ |z - z_{f0}| > d \end{cases}. \tag{2.2.6}$$

where d is the travel distance of peristalsis, and l is set as $0.1d$. The function $H(t, \Delta t)$ provides the remainder in the division of t by Δt, which indicates that peristalsis is a periodic motion. The coefficient c in the last term in Eq.(2.2.3) indicates the speed of long-term contraction. Since the amplitude of long-term contraction varies significantly, its effect is expressed by changing c. The values of these parameters are discussed in section "Parameters"and provided in Table 2.1.

2.2.2 Numerical methods

Digested chyme was assumed to be an incompressible and Newtonian fluid. The continuity equation, *i.e.*, conservation of mass, and the Navier-Stokes equation, *i.e.*, conservation of momentum, were solved numerically under the given boundary conditions. By assuming the density of fluid to be $\rho = 1000$ kg/m^3 and the viscosity to be $\mu = 10^{-3}$ Pa·s, similar to the values of water, the Reynolds number defined by Re= $\rho W U_c/\mu$ is smaller than 0.01. Thus, the flow can be regarded as inertia-free. Even if a higher viscosity of the digested chyme is assumed, the streamlines

and diffusivities are unchanged, although the pressure and shear stress in the intestine increase proportionally with the viscosity, provided that the wall boundary conditions is prescribed by the velocity as in this study.

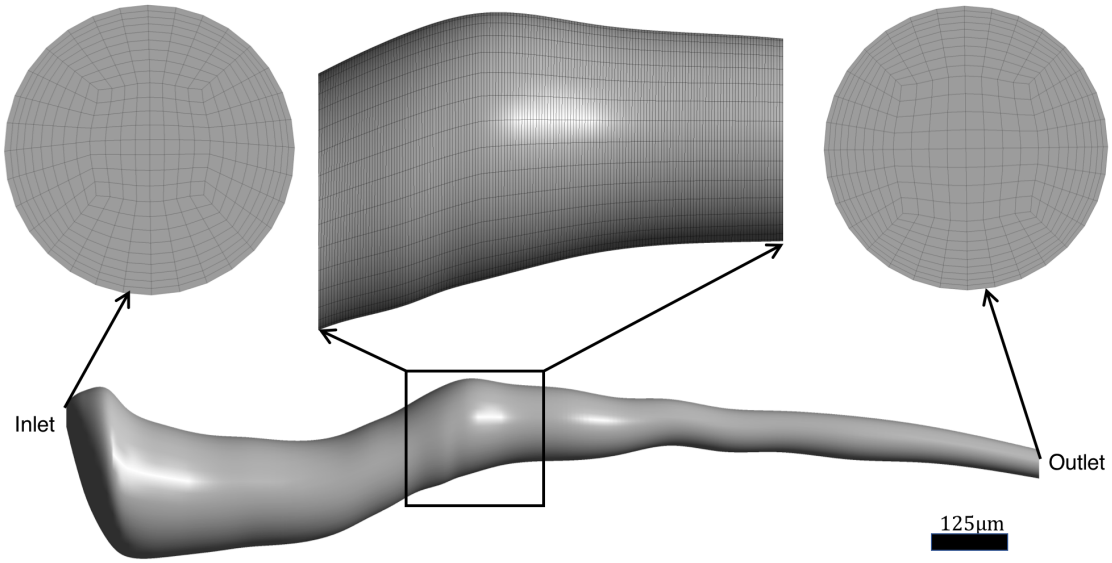

Figure 2.3. A structure mesh model of the intestine of a zebrafish larva at 7 days ($t = 0$ h).

In the study by Field et al.[18], injected fluorescent fluid was gradually pushed downstream, because a certain volume of fresh water flowed into the intestine through the esophagus even in the absence of feeding. The inflow rate was calculated as follows. In Field et al.[18], the injected fluid initially occupied volumeV_1^0 with the fluorescent intensity of I_1^0. After 24 h of observation, some of the fluorescent fluid was exhaustedrom the anal, and the total fluorescent intensity of the intestine decreased to I_{sum}^{24} . By assuming a linear correlation between the fluorescent intensity and the volume of the fluorescent fluid, one can estimate that the volume of fluorescent fluid remained in the intestine for 24 h was $V_1^0 \times \frac{I_{sum}^{24}}{I_1^0}$. Thus, the average inflow rate for 24 h may be calculated as $Q_0 = \left(V_{sum}^{24} - V_1^0 \times \frac{I_{sum}^{24}}{I_1^0} \right) / (24 \times 60 \times 60) = 8.3 \times 10^{-17}$ m^3/s, where V_{sum}^{24} is total volume of intestine after 24 h. In the present study, the flow rate at the inlet of the intestine was varied from 0 to 5 Q_0, and a parabolic velocity profile was assumed at the inlet. At the outlet, the relative pressure was

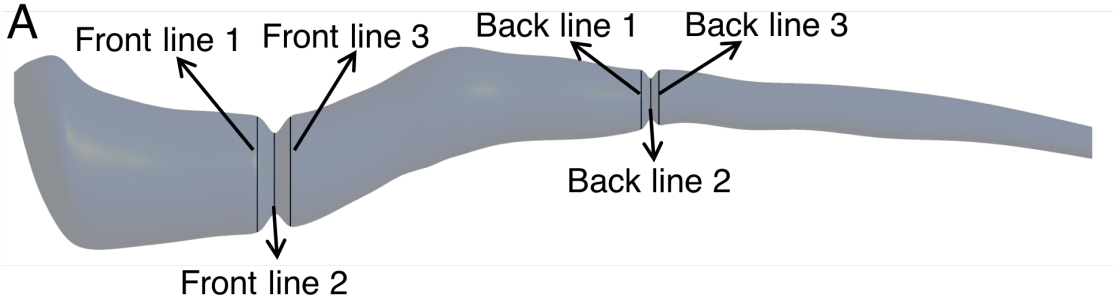
A
Front line 1
Front line 3
Back line 1
Back line 3
Back line 2
Front line 2

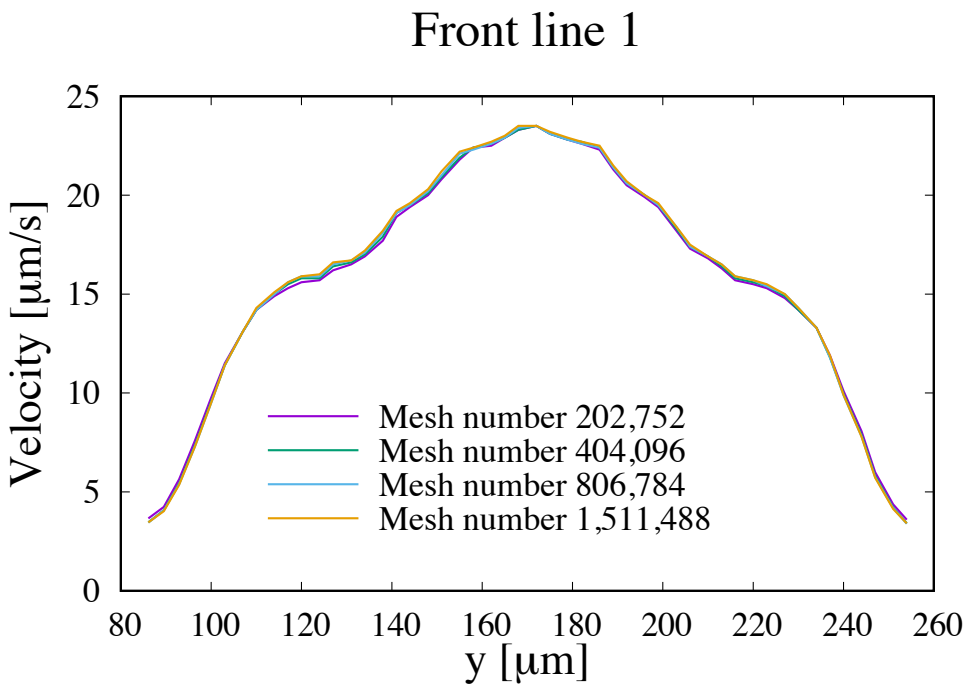
Front line 1
Velocity [μm/s]
y [μm]
Mesh number 202,752
Mesh number 404,096
Mesh number 806,784
Mesh number 1,511,488

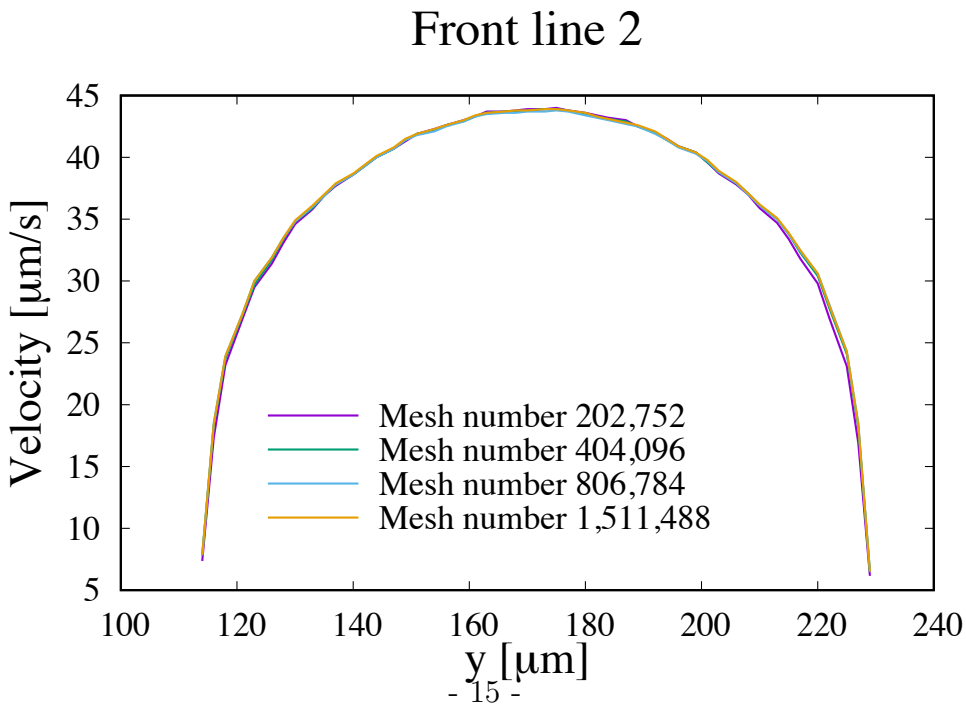
Front line 2
Velocity [μm/s]
y [μm]
Mesh number 202,752
Mesh number 404,096
Mesh number 806,784
Mesh number 1,511,488

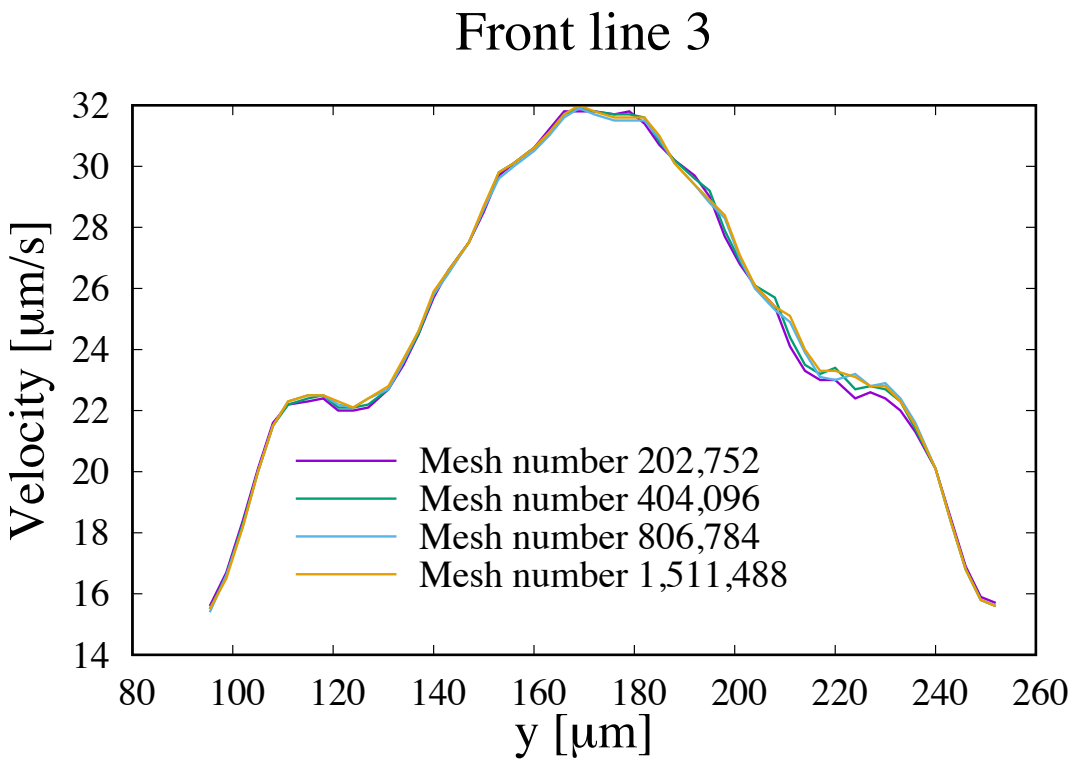
Front line 3
Velocity [μm/s]
y [μm]
Mesh number 202,752
Mesh number 404,096
Mesh number 806,784
Mesh number 1,511,488

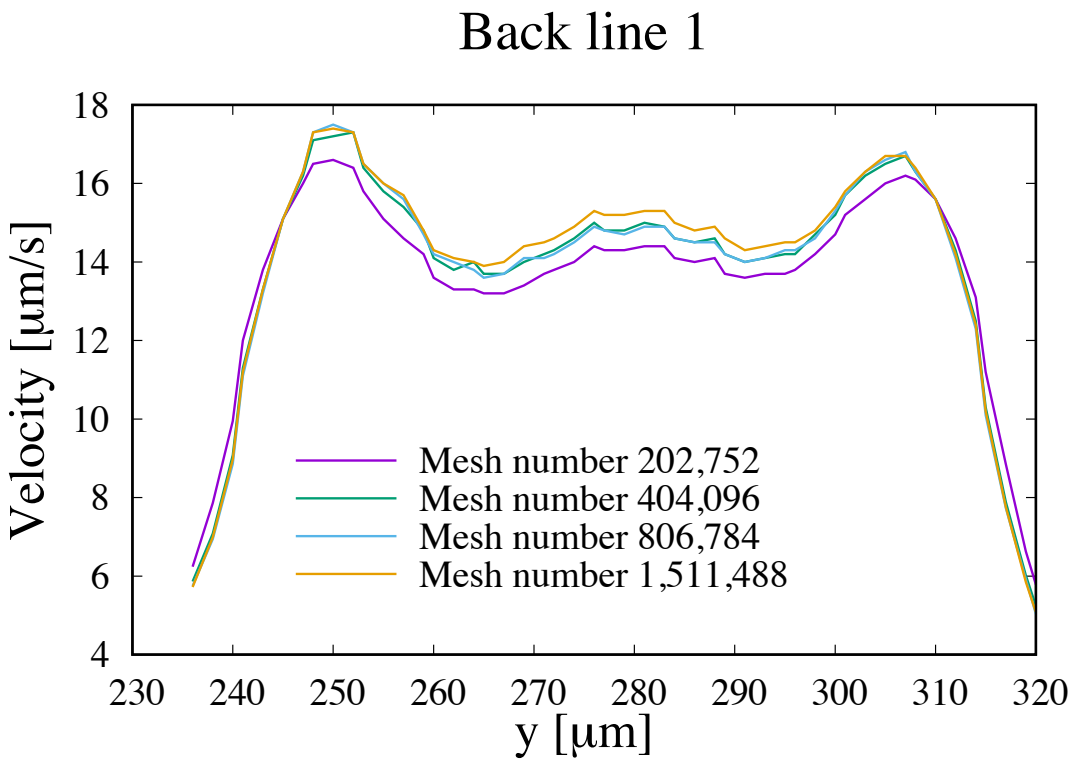
Back line 1
Velocity [μm/s]
y [μm]
Mesh number 202,752
Mesh number 404,096
Mesh number 806,784
Mesh number 1,511,488

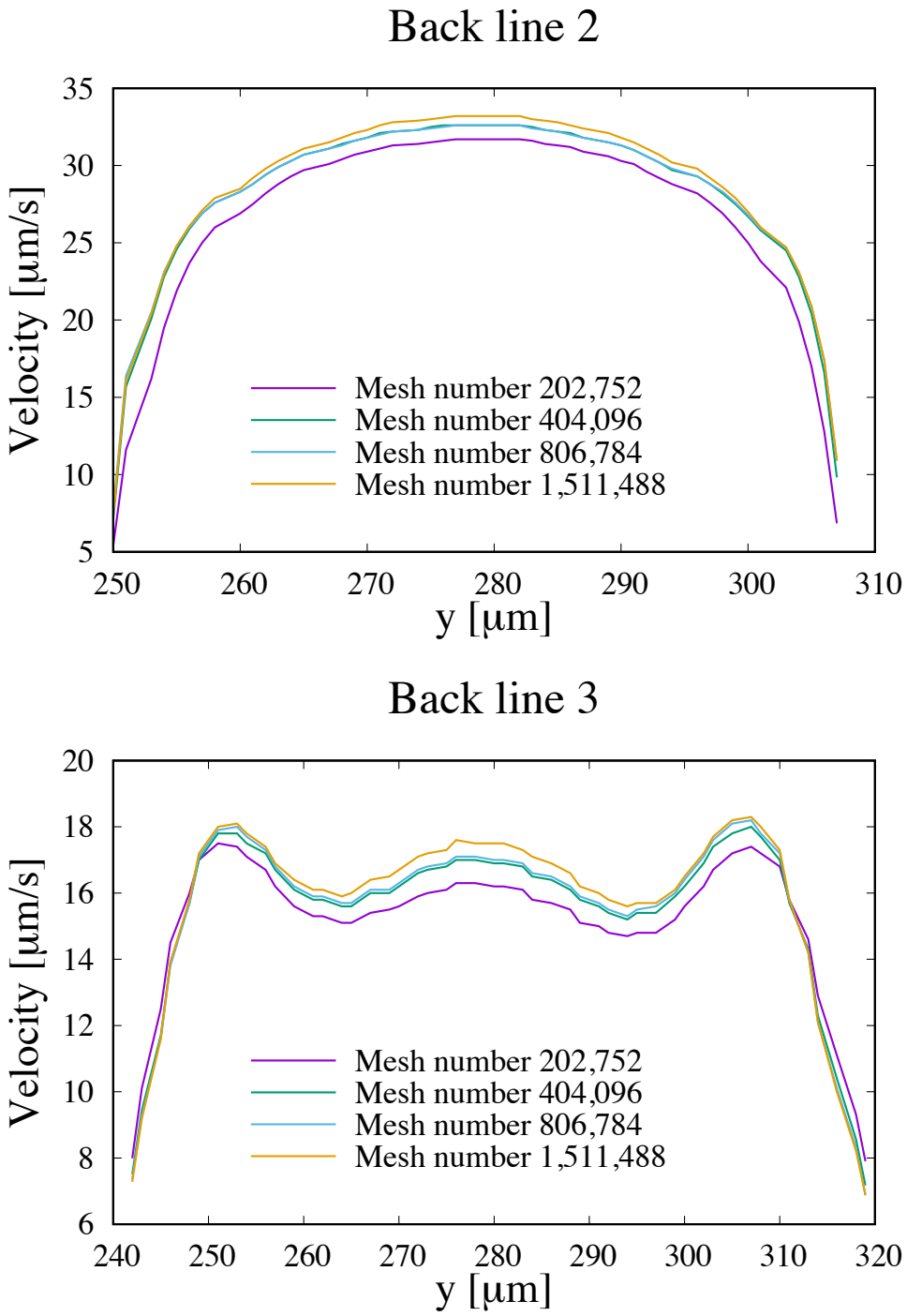

Figure 2.4. A velocity distribution of four cases(202752,404096,806784 and 1511488 mesh element) at different location for checking mesh model of the intestine of a zebrafish larva at 7 days ($t = 0$ h). A: the location of selected lines for the mesh checking. The lines were on the lateral cross-section between the narrows. Front mean the narrow on the anterior intestine, back mean the narrow on the posterior intestine.

assumed to be zero, because the anal of 7 dpf larvae is open to the surrounding fluid. On the wall, radial velocity was prescribed by taking the time derivative of Eq.(2.2.3), and no axial velocity was assumed.

The governing equations with the boundary conditions were solved using the commercial software ANSYS-CFX 16.2 (ANSYS, USA),which the license was bought by our lab . The mesh convergence tests were performed a priori, and a structured mesh with 404,096 hexahedra elements and 423,981 nodes was used as Figure2.3 and Figure2.4. In order to decrease the time cost, the mesh model with 404,096 was selected for real simulation.This treatment allows us to perform parametric study for a wide range of parameters. It was confirmed that the mesh did not considerably influence the results. An moving wall,transient analysis type,10^{-4} target levels of root mean square residual were set in the CFX software in this chapter. And 10^{-5} target levels of root mean square residual was set in next chapter for the transport phenomena.

After obtaining the flow field, the trajectories of fluid particles were calculated by integrating velocity with time. In section "Mixing induced by retrograde peristalsis" , the dispersion coefficient [28, 57] is calculated to evaluate the mixing effect, which is defined as:

$$D(t) = \frac{1}{N}\sum_{i=1}^{N}\frac{[\mathbf{x}_i(t) - \mathbf{x}_i(0)]^2}{6t} \tag{2.2.7}$$

where $\mathbf{x}_i$ is the three-dimensional position of the ith particle. The trajectory of the ith particle was calculated by integrating velocity $\mathbf{u}$ with time:

$$\mathbf{x}_i(t_2) = \mathbf{x}_i(t_1) + \int_{t_1}^{t_2}\mathbf{u}_i dt \tag{2.2.8}$$

The total number of particles N was set as 100 in this study, and five independent calculations with different initial positions were performed. When the value of D converges over time, D is equivalent to the diffusion coefficient.

2.2.3 Parameters

The parameters used in this study are listed in Table 2.1. Based on the observations by Holmberg et al.[24] and Roach et al.[54], the depth of contraction δ_f was varied from 10 to 50 of the radius of the intestine. The propagation velocity of peristalsis

(U_c) was assumed to be 30 µm/s. The interval time (Δt) was assumed to be 23 and 57 s for retrograde and anterograde peristaltic motion, respectively. The travel distance of peristalsis was assumed to be 350 µm/s for retrograde peristalsis (d_{re}) and 700 µm/s for anterograde peristalsis (d_{an}). To discuss the function of the intestine, results are shown for δ_f= 0.1–0.5 R, Q_{in}= 0–5 Q_0, c = 0–40, and h = 0–24 h.

Table 2.1. Parameter used in Chapter 2

Parameters for peristaltic motion and geometry		
Depth of peristaltic contraction δ_f	0.1 –0.5R	R is the radius (R=W/2)
Time interval of peristaltic waves ΔT	ΔT_{re}=23 s ΔT_{an}=57 s	Holmberg et al.[24], Roach et al.[54]
Travel distance of retrograde peristalsis d_{re}	350 µm	Roach et al.[54], Holmberg et al.[24]
Travel distance of anterograde peristalsis d_{an}	700 µm	Roach et al.[54], Holmberg et al.[24]
Half width of the peristaltic wave λ_f	$0.5\delta_f$	Baker et al.[1]
Origin of peristaltic wave generation z_{f0}	645 µm	Roach et al.[54], Holmberg et al.[24]
Amplitude of the initial expansion of the intestine δ_g	90 µm	Determined by comparing with Field et al.[18]
Relaxation time of the long-term contraction τ_g	5.6 h	Determined by comparing with Field et al.[18]
Half-width of the initial expansion λ_g	650 µm	Determined by comparing with Field et al.[18]
Position of the initial expansion z_{g0}	40 µm	Determined by comparing with Field et al.[18]
Coefficient for controlling the speed of the long-term contraction c	0, 1, 5, 10, 20, 30, 40	
Flow parameters		
Propagation velocity of the peristaltic wave U_c	30 µm/s	Holmberg et al.[24]
Fluid density ρ	1000 kg/m^3	
Fluid viscosity μ	0.001 Pa·s	
Volume flow rate at the inlet Q_{in}	0 –5 Q_0	Field et al.[18] Q_0=8.3×10^{-17}m^3/s

2.3 Results

2.3.1 Mixing induced by retrograde peristalsis.

The effect of retrograde peristalsis on the mixing function in the upstream portion of the intestine, *i.e.*,$z < z_{f0}$, was investigated first. Figure 2.5A shows the velocity vectors around the retrograde peristaltic wave under the conditions $t = 5$ s, $Q_{in} = 1\ Q_0, \delta_f = 0.3$ R, $c = 0$, and $h = 0$ h. Jet flow was generated at the narrowing, and large radial velocities were induced upstream and downstream of the narrowing. Figure 2.5B shows the trajectories of particles, initially aligned perpendicularly to the z-axis, during one period of peristalsis. The particles moved a considerable distance during the period, which may result in mixing.

To discuss the mixing effect quantitatively, the dispersion coefficient defined by Eq.(2.2.7) was calculated using the trajectories of particles in the upstream portion of the intestine. The values of D under the conditions of $Q_{in} = 1\ Q_0, \delta_f = 0.3$ R, $c = 0$ and $h = 0$ h are shown in Figure 2.6. The value of D increased rapidly until 400 s, and the fluid particles exhibited ballistic motion. After 1000 s, the value of D stabilized but decreased gradually thereafter. Due to the long-term contraction described by Eq.(2.2.1), approximately 10 % of the contents were excreted through the outlet over a 30 min period. Therefore, the dispersion coefficient over 30 min (1800 s) is appropriate to describe the mixing function of the zebrafish intestine. The value of D was in the order of 10^{-12} m^2/s.

A parametric study was performed next. Figure 2.7A shows that the inlet flow rate Q_{in} enhanced the degree of mixing. The difference between 0 and 1 Q_0 was greater than that between 1 Q_0 and 5 Q_0, which indicates that a small amount of inflow exerted a dramatic effect on the mixing function. Figure 2.7B shows the effect of the depth of peristaltic constriction, δ_f. The effect of δ_f was not significant, although it resulted in a slight increase in D at $t = 2300$ s. Since the flow in the intestine was inertia-free, the speed of the jet flow at the narrowing did not play a major role in the mixing. This might explain why the effect of δ_f was not significant. Figure 2.7C shows the effect of the geometry of the intestine at various times after feeding h. The value of D decreased as h increased, because as h increased, the

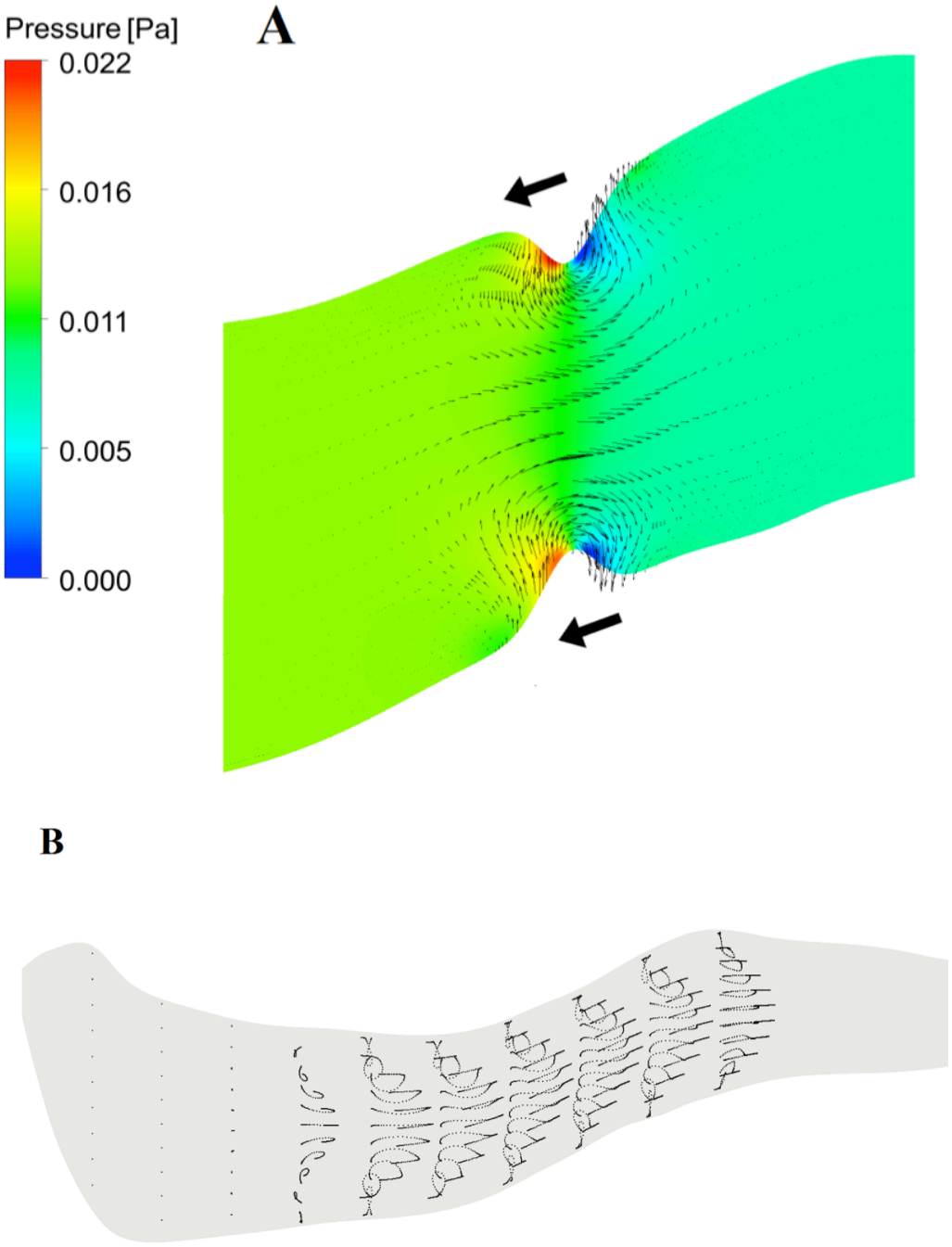

Figure 2.5. Flow field induced by retrograde peristalsis under the conditions $Q_{in} = 1$ Q_0, $\delta_f = 0.3$ R, $c = 0$ and $h = 0$ h. A: Velocity vectors and pressure distribution around the narrowing at 5 s. The arrow shows the direction of wave propagation. B: Trajectories of one hundred particles initially placed perpendicularly to the z-axis during one period of peristalsis.

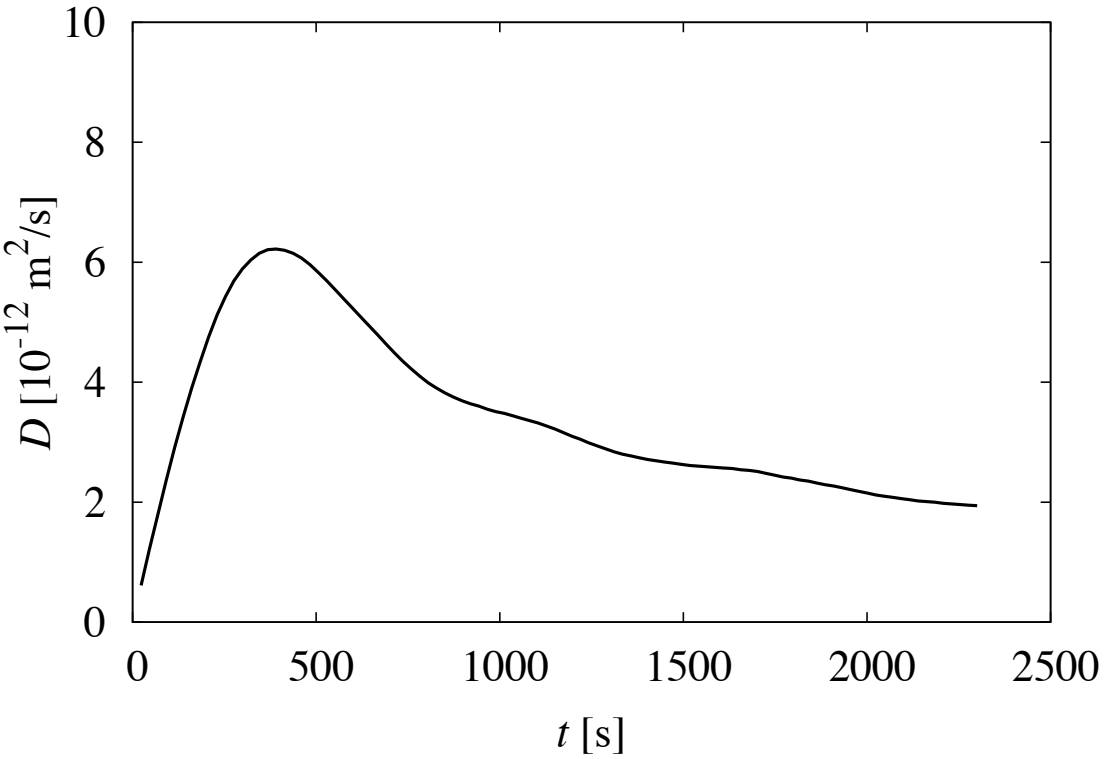

Figure 2.6. Change in the dispersion coefficient D over time under the conditions Q_{in} = 1 Q_0, δ_f = 0.3 R, c = 0 and h = 0 h.

volume of the intestine decreased, and thus the space within which fluid particles could spread was reduced.

2.3.2 Pumping induced by anterograde peristalsis.

The effect of anterograde peristalsis on the pumping function was investigated. Figures 2.8A and 2.8B show the pressure distribution with and without anterograde peristalsis, respectively, under the conditions t = 5 s, Q_{in} = 1 Q_0, δ_f = 0.3 R, c = 20 and h = 0 h. A value of c = 20 was used, because anterograde peristalsis is sometimes accompanied by a strong contraction of the entire intestine. The pressure decreased significantly in the presence of anterograde peristalsis. The pressure decrease was generated at the narrowing (Figure 2.8C), where inverse flow towards the inlet was generated, although the bulk flow was towards the outlet. In the field of mechanical engineering, a pump generates a pressure difference between the inflow and outflow. In the zebrafish intestine, the outlet was open to the surrounding fluid

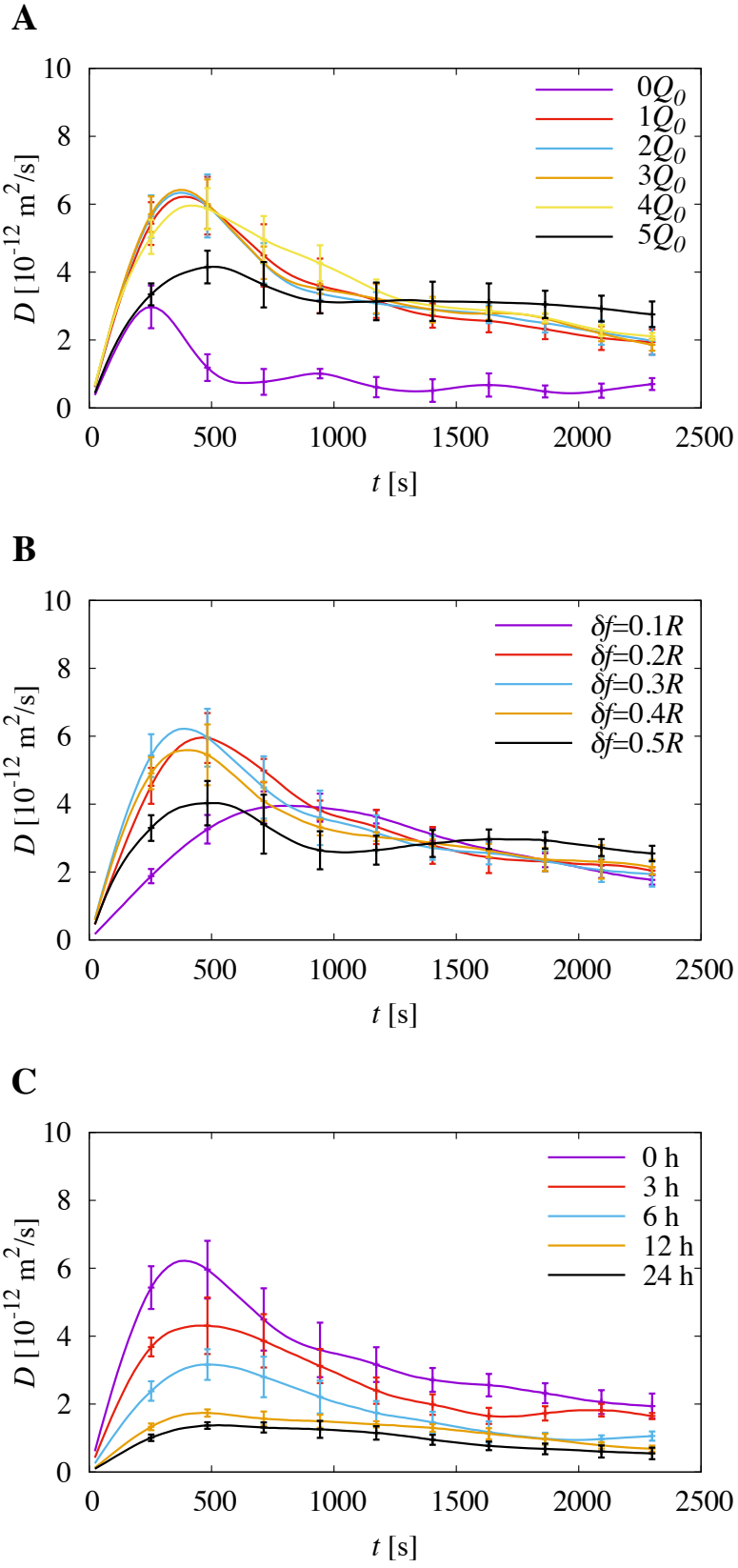

Figure 2.7. Effects of various parameters on the dispersion coefficient:Q_{in}(δ_f = 0.3 R, c = 0 and h = 0 h) (A), δ_f(Q_{in} = 1 Q_0, c = 0 and h = 0 h) (B) and h (Q_{in} = 1 Q_0, δ_f = 0.3 R and c = 0) (C)

and had zero relative pressure. Thus, the pressure at the inlet side of the narrowing decreased. Because the pressure decrease is a reasonable measure of the pumping function, it is analyzed below.

Figure 2.9A shows the instantaneous pressure distribution along the dorsal line of the intestinal wall under the same conditions as in Figures 2.8A and 2.8B. Again, the pressure was decreased significantly by anterograde peristalsis. The pressure at the inlet side of the narrowing was 0.005 Pa less than that at the outlet side, although the pressure oscillated due to flow around the narrowing. By calculating the average of the pressure over one period of peristalsis, the time-average pressure distribution $Pa(z)$ can be obtained as shown in Figure 2.9B. The time-average pressure at the inlet side of the intestine was reduced by 0.003 Pa, which may considerably reduce the work to generate peristaltic motion.

Next, a parametric study was conducted. To discuss the pumping effect, the average pressure of the intestine, P_t , was defined as the spatial average of $Pa(z)$ over the surface of the intestinal wall. Figure 2.10A shows the effect of the long-term contraction coefficient c on P_t. The pressure increased with increasing c, because the flow towards the outlet was increased by the large long-term contraction. The effect of anterograde peristalsis on P_t was evident irrespective of the value of c. Figure 2.10B shows the effect of the inflow rate Q_{in}. The effect was limited, because Q_{in} was not much greater than the flow rate generated by long-term contraction $g(z,t)$. Figure 2.10C shows the effect of the depth of peristaltic constriction δ_f; the pressure decreased markedly with increasing δ_f. Although δ_f had little effect on mixing (cf. Figure 2.7B), it made a considerable contribution to the pumping function. Figure 2.10D shows the effect of the geometry of the intestine at various times after feeding h. The effect of h was limited, and the pressure decreased irrespective of its value.

2.4 Discussion

We first discuss the significance of the mixing induced by retrograde peristalsis (cf. section “Mixing induced by retrograde peristalsis”). Within the intestine, chemical substances and small particles diffuse as a result of Brownian motion. The Stokes-Einstein equation for a spherical particle can be used to discuss the order

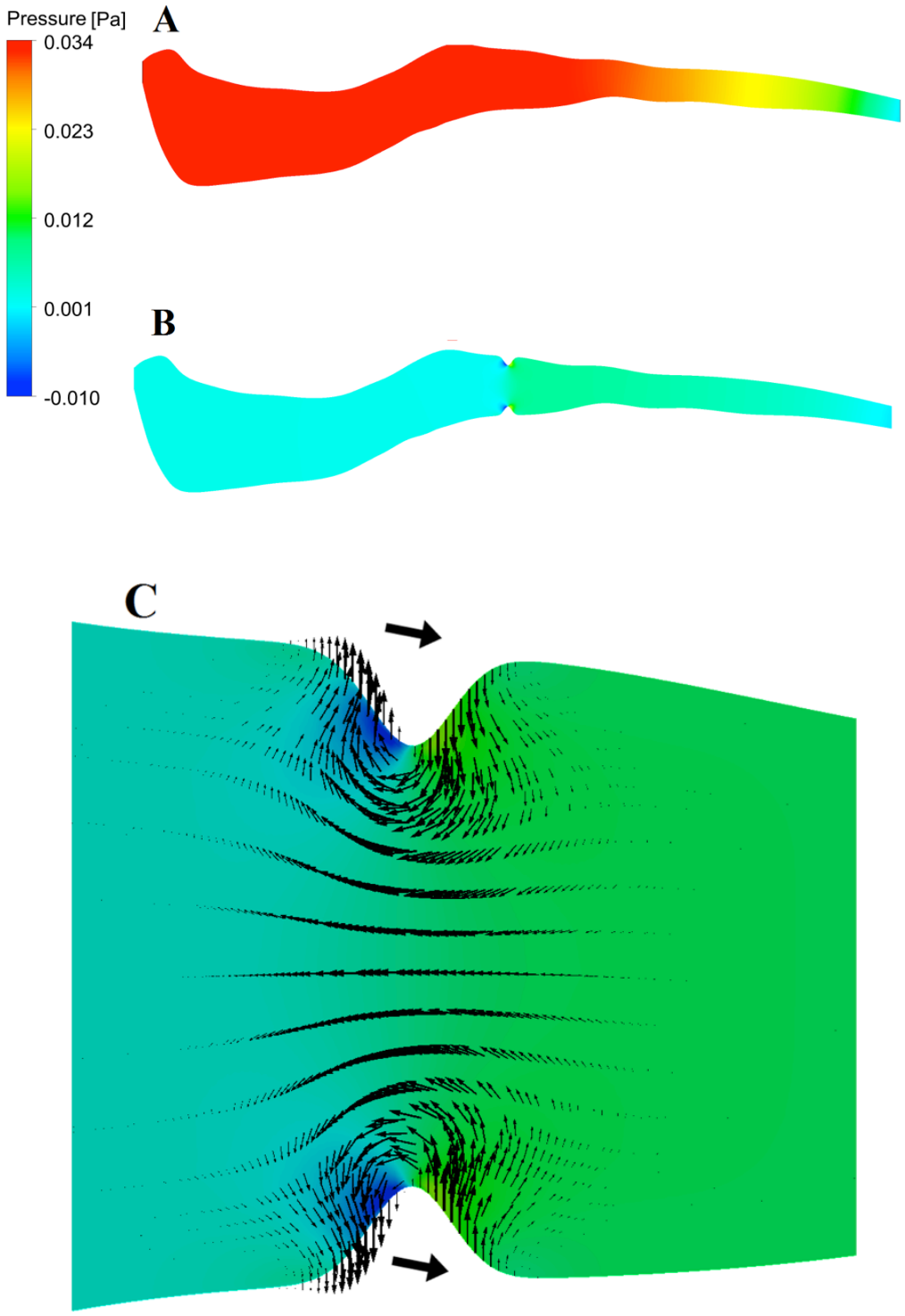

Figure 2.8. . Pressure distribution under the conditions $t = 5$ s, $Q_{in} = 1\ Q_0$, $\delta_f = 0.3$ R, $c = 20$ and $h = 0$ h. A: Pressure distribution in the absence of anterograde peristalsis. B: Pressure distribution in the presence of anterograde peristalsis. C: Velocity vectors and pressure around the narrowing. The arrow shows the direction of wave propagation.

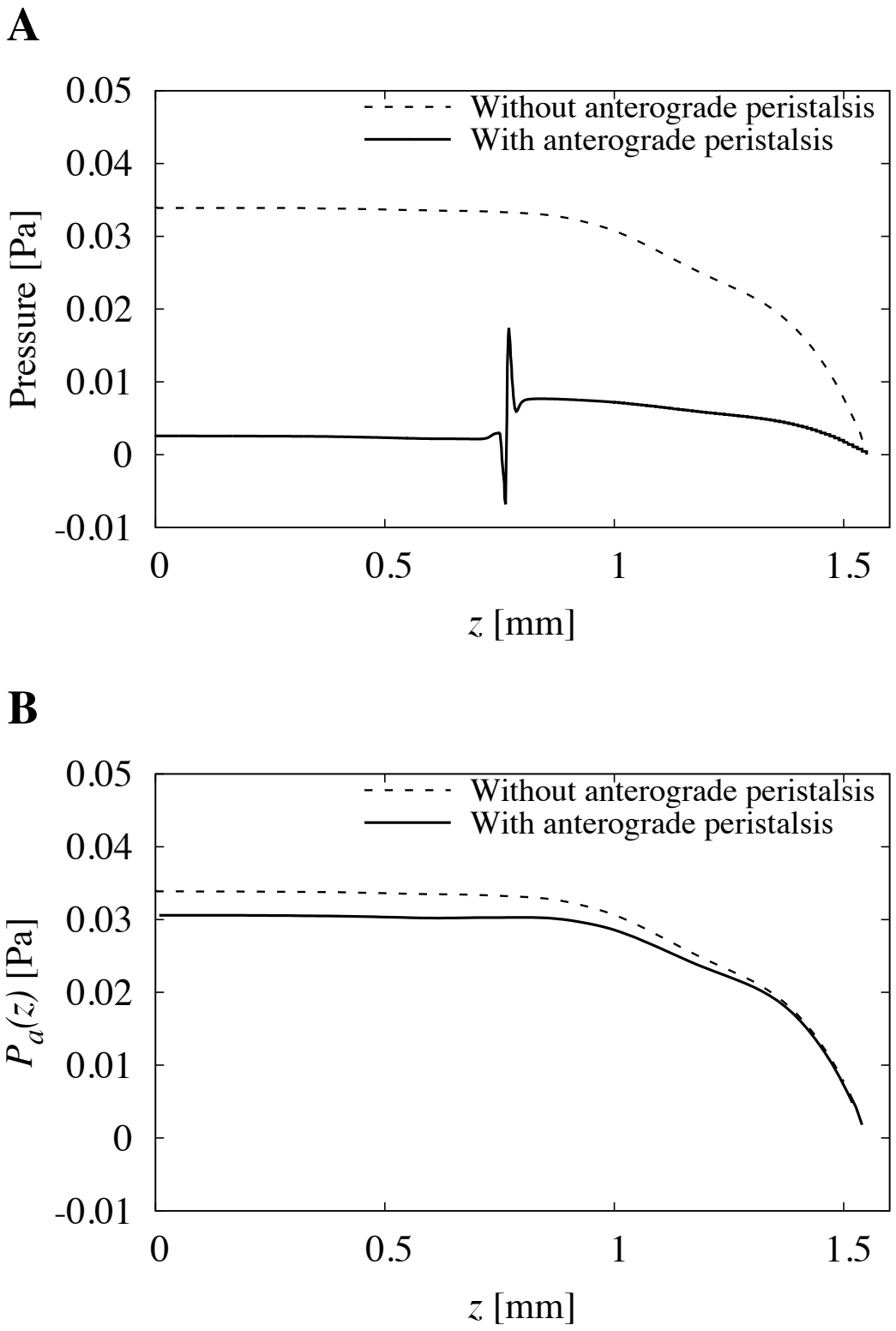

Figure 2.9. Pressure distribution with or without anterograde peristalsis under the conditions $Q_{in} = 1\ Q_0$, $\delta_f = 0.3$ R, $c = 20$ and $h = 0$ h. A: The instantaneous pressure distribution along the dorsal line of the intestinal wall at 5 s. B: The time-average pressure distribution $Pa(z)$ calculated as the average pressure during one period of peristalsis.

A

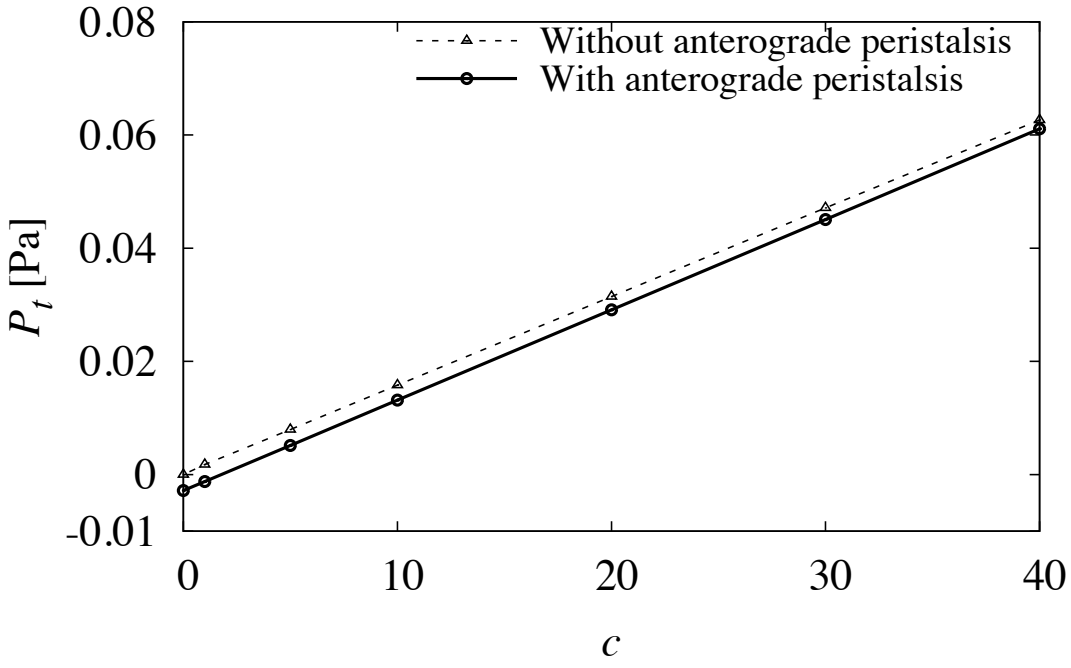
0.08
0.06
0.04
0.02
0
-0.01
P_t [Pa]
0
10
20
30
40
c
Without anterograde peristalsis
With anterograde peristalsis

B

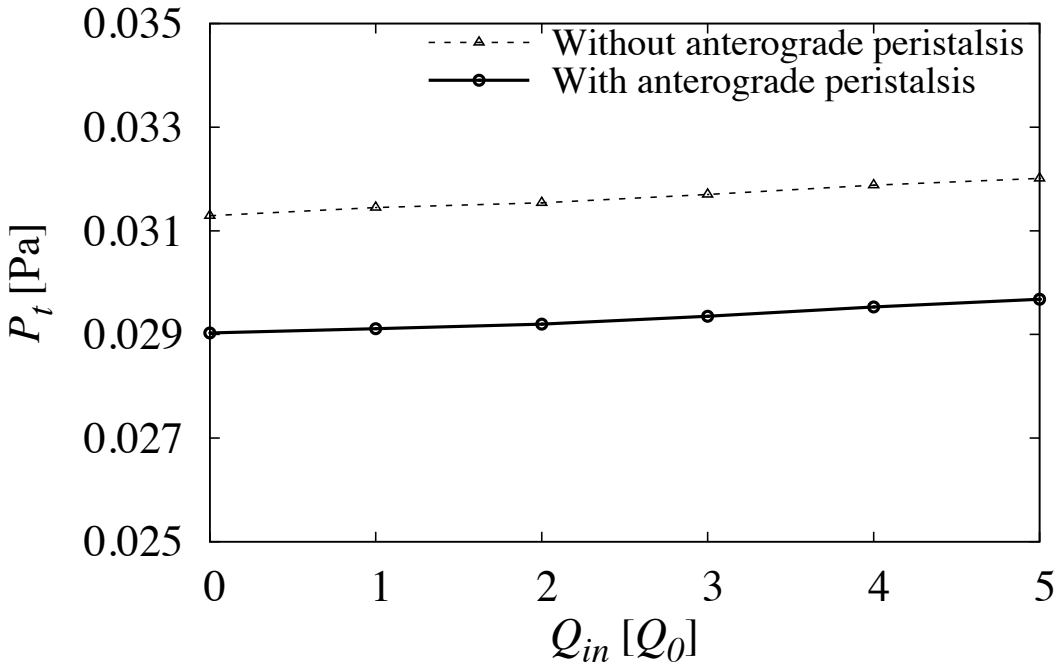
0.035
0.033
0.031
0.029
0.027
0.025
P_t [Pa]
0
1
2
3
4
5
Q_{in} [Q_0]
Without anterograde peristalsis
With anterograde peristalsis

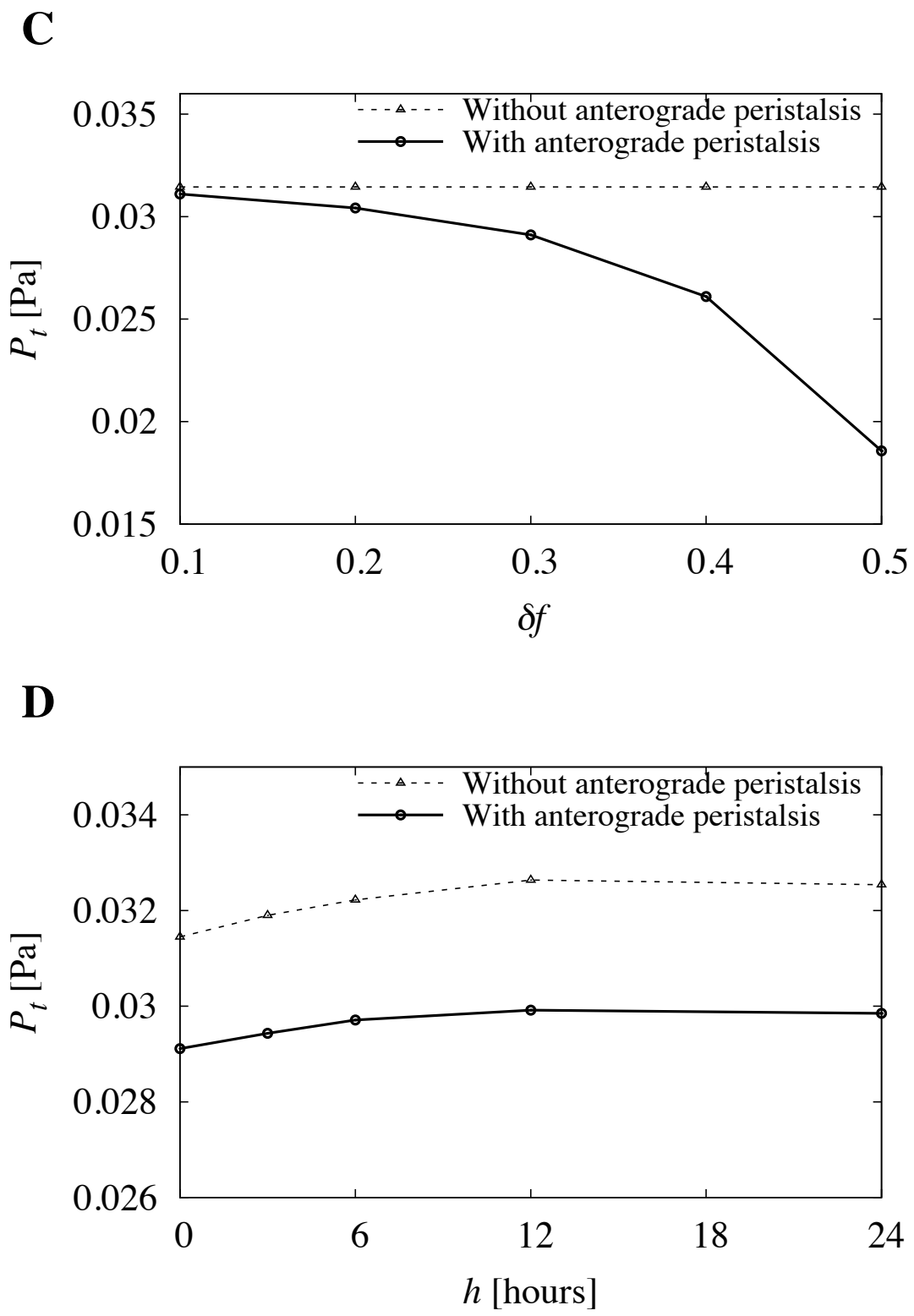

Figure 2.10. Effects of various parameters on the average pressure of the intestine P_t calculated as the average pressure on the surface of the intestinal wall during one period of peristalsis: c ($Q_{in} = 1\ Q_0$, $\delta_f = 0.3$ R and $h = 0$ h) (A), Q_{in} ($\delta_f = 0.3$ R, $c = 20$ and h = 0 h) (B), δ_f($Q_{in} = 1\ Q_0$, $c = 20$ and $h = 0$ h) (C) and h ($Q_{in} = 1\ Q_0$, $\delta_f = 0.3$ R and $c = 20$) (D).

of Brownian diffusion D_B, which is defined as $D_B = k_B T/(6\mu r)$, where k_B is the Boltzmann constant, T is the temperature, μ is the viscosity, and r is the radius. At a temperature of 37 °C and viscosity of 0.001 Pa·s, D_B is in the order of 10^{-12} m^2/s for a particle 0.4 µm in diameter. Since D due to retrograde peristalsis was in the order of $10^{-12} m^2/s$, the mixing of particles smaller than 0.4 µm would be attributed mainly to Brownian motion, and that of those larger than 0.4 µm to retrograde peristaltic motion. If the digested chyme has a higher viscosity, e.g., 1 Pa·s, the dispersion coefficient is unaffected due to the inertia-free nature of the flow field. In contrast, Brownian diffusivity decreased to 1/1000, as determined by the Stokes-Einstein equation. Therefore, the dispersion of particles caused by retrograde peristalsis may be more important than that caused by Brownian diffusion, even for those particles 0.4 µm in diameter.

Finally, the effect of the pressure decrease caused by anterograde peristalsis (cf. section "Pumping induced by anterograde peristalsis") on energy expenditure by the intestinal muscle is discussed. The activation and maintenance heat of muscle can be calculated by the equation $H_{AM} = A_0 + M_0\sigma_S/\sigma_0$ [25, 47, 48, 62], where A_0 is the activation heat of muscle, M_0 is the coefficient of the maintenance heat, σ_0 is the maximum tension of the muscle, and σ_s is the muscle tension. The muscle tension σ_s can be assumed to be proportional to the pressure in the intestine, because the muscle contraction force should balance the resistance caused by the digested chyme and surrounding tissues. Therefore, the pressure decrease caused by anterograde peristalsis is beneficial in terms of reducing the energy consumption by the intestinal muscle.

In this study, we tried to reproduce the experiment done by Fieldet al.[18], in which small amount of powdered feed and fluorescent tracer particles were added to deionized water. In order to mimic the experimental condition in the present paper, we assumed that the fluid in the intestine was Newtonian with the viscosity of 10^{-3} Pa·s. In nature, however, the fluid in the intestine may have different rheological properties from water. When the fluid is Newtonian but with much higher viscosity, the pressure drop due to the peristalsis increases linearly with the viscosity. The dispersion coefficient, on the other hand, does not change. This is because the flow in the intestine is Stokesian, and the velocity field is unaffected by the viscosity under

the present boundary conditions. When the fluid shows non-Newtonian properties, the linearity in the flow field breaks down, and complex phenomena may come out. Since rheological properties of the fluid in the intestine of zebra fish larvae were not found in literature, we would like to investigate the effects in our future studies.

2.5 Summary

We proposed an anatomically realistic three-dimensional geometric model of the zebrafish larval intestine, and then investigated the transport phenomena caused by peristaltic motion with numerical simulation method. The results showed that retrograde peristaltic motion was the major contributor to the mixing function. The dispersion caused by peristalsis over 30 min was in the order of 10^{-12} m^2/s, which is greater than the Brownian diffusion of a sphere of 0.4 µm diameter. In contrast, anterograde peristaltic motion contributed mainly to the pumping function. The pressure decrease due to peristalsis was in the order of millipascals, which may reduce the activation and maintenance heat of intestinal muscle. These findings enhance our understanding of the mixing and pumping functions of the intestine of zebrafish larvae.

Chapter 3

Bacterial spatial heterogeneity in the intestine of zebrafish larvae

3.1 Introduction

Trillions of microorganisms thrive within the intestines of humans or other animals, most of which are bacteria that have a symbiotic relationship with the host and play an important role in the health of the host. Some intestinal bacteria are sources of inflammation and infection, and are implicated in gastrointestinal and other diseases such as obesity, colon cancer, opportunistic infections, and inflammatory bowel disease [21, 22, 31, 37, 44]. Hence, many investigations of intestinal bacteria have been conducted over the last decade. Some of these studies focused on the heterogeneous distribution of bacteria within the intestine. Donaldson et al.[13] investigated the biogeography of bacteria in the gut and the relevance of spatial heterogeneity to health and disease. Lee et al.[36] visualized microbial biogeography within the colon, and noted that the niche within colonic crypts represented a reservoir of bacteria to maintain long-term colonization. Bacterial distribution has also been investigated in physical terms [15, 56], but a comprehensive understanding of intestinal bacterial flora is still lacking.

Zebrafish larvae have been widely employed as a model organism in studies of vertebrate biology due to their transparency and the similarity of their major organs to those of humans [39, 40]. Bacterial flora has also been studied in the intestines of zebrafish by many researchers [2, 29, 49, 55, 71]. Recently, Jemielita et al.[29] reported that *Aeromonas* bacteria in the larval zebrafish intestine exhibit a heterogeneous distribution and are aggregated in the middle of the intestinal tract.

Wiles et al.[71] further investigated the distribution of *Aeromonas* by introducing another bacterium, *Vibrio*, into the larval zebrafish intestine. They showed that the habitat of *Aeromonas* was modified by competition with *Vibrio*, resulting in altered distribution. Although the heterogeneous distribution of intestinal bacteria is important biologically and clinically, its mechanism remains largely unknown.

Mathematical modeling can be useful for elucidating the heterogeneous distribution of bacteria, as it can provide clear structure for complex phenomena through well-defined numerical experiments. Mathematical models of bacterial flora in the intestine have been reported by Ishikawa et al.[27] and Cremer et al.[9]. However, these models of the intestine were too idealized, and thus their results cannot be used to analyze the heterogeneous distribution of bacteria within the intestine. To the best of our knowledge, no mathematical model has yet been developed to describe this phenomenon.

In this study, we introduce a computational model to describe the heterogeneous distribution of bacteria in the intestines of zebrafish larvae. An anatomically-realistic three-dimensional geometric model of the larval zebrafish intestine was constructed based on experimental data from Jemielita et al.[29], and the equations governing fluid mechanics, nutrient transport, and growth of a single strain of bacteria were solved numerically. We also employed a scaling argument in the Discussion, in which we showed that the taxis velocity of bacteria must be larger than the sum of the diffusive velocity and the background bulk flow velocity to induce bacterial aggregation.

3.2 Modeling and Methods

3.2.1 Geometry of the intestine

A three-dimensional model of the intestine was constructed in a similar manner to that described in our previous study [72]. The centerline and width of the intestine of a larval zebrafish at 5 days post-fertilization[29] were extracted with the image analysis software ImageJ (NIH, USA). The origin of coordinates was set at the inlet of the intestine, i.e., just past the esophageal sphincter, and the z-axis was defined as the direction toward the outlet, as shown in Figure 3.1. Considering previous experimental observations [1, 3, 54], the cross-section of the intestine was assumed

to be circular, and bilateral symmetry of the intestinal tract was assumed.

Two types of peristaltic motion were considered: retrograde peristalsis that propagates toward the inlet, and anterograde peristalsis that propagates toward the outlet. Both peristaltic waves originate immediately distal of the end of the swim bladder at z_{f0} [24, 54]. Superimposing the two types of peristaltic motion given by $f(z,t)$ in a manner similar to that of Ishikawa et al.[27]and Yang et al.[72], the diameter of the intestine, $W(z,t)$, was determined via:

$$\begin{cases} W(z,h+t) = W_0(z,h) + f_{an}(z,t) + f_{re}(z,t), \\ f_{an}(z,t) = -\delta_f J(z,d_{an}) exp\left[\dfrac{ln0.5}{\lambda_f^2}\{z - H(t,\Delta t_{an})U_c - z_{f0}\}^2\right], \\ f_{re}(z,t) = -\delta_f J(z,d_{re}) exp\left[\dfrac{ln0.5}{\lambda_f^2}\{z - H(t,\Delta t_{re})U_c - z_{f0}\}^2\right], \end{cases} \tag{3.2.1}$$

where $W_0(z)$ is the diameter of the intestine without peristalsis, and $f_{an}(z,t)$ and $f_{re}(z,t)$ are constrictions generated by anterograde and retrograde peristaltic motion, respectively. δ_f is the depth of the peristaltic waveform, λ_f is the half-width, and U_c is the wave propagation velocity. The function $J(z,d)$ was used to express the gradual dissipation of peristalsis, and is defined as:

$$J(z,d) = \begin{cases} 1, & when\ |z - z_{f0}| \le d \\ exp[-\dfrac{(|z - z_{f0}| - d)}{l}], & when\ |z - z_{f0}| > d \end{cases}. \tag{3.2.2}$$

where d is the peristalsis travel distance, and l is set to 0.1 d. The function $H(t,$ $\Delta t)$ provides the remainder in division of t by Δt, which indicates that peristalsis is a periodic motion. The values of these parameters are discussed in the section "Parameters"and provided in Table 3.1.

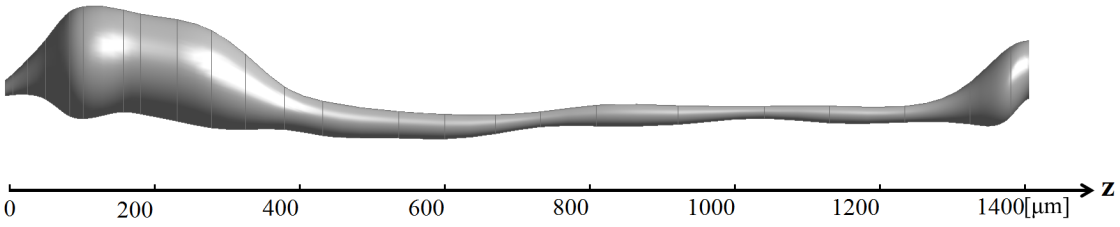

Figure 3.1. Three-dimensional model of the intestine of a zebrafish larva at 5 days post-fertilization based on experimental data in Jemielita et al.[29] Bilateral symmetry is assumed.

3.2.2 Basic equations and boundary conditions of fluid mechanics

We resolved the flow of incompressible and Newtonian fluids in the zebrafish intestine. The continuity equation and the Navier-Stokes equation are given as:

$$\begin{cases} \nabla \cdot \mathbf{u} = 0, \\ \\ \dfrac{\partial \mathbf{u}}{\partial t} + (\mathbf{u} \cdot \nabla)\mathbf{u} = -\dfrac{1}{\rho}\nabla p + \dfrac{\mu}{\rho}\nabla^2 \mathbf{u} \end{cases} . \tag{3.2.3}$$

where $\mathbf{u}$ denotes the velocity vector, ∇ is the gradient operator, ρ is the density, p is the pressure, and μ is the viscosity. We set the density of the fluid to ρ = 1000 kg/m^3 and the viscosity to μ=10^{-3} Pa·s, assuming the fluid in the zebrafish intestine is similar to the surrounding water. Because the Reynolds number,defined as Re=$\rho W U_c/\mu$, was smaller than 0.01, the flow in the intestine could be approximated as inertia-free. The flow rate at the inlet of the intestine was varied from 0 to 5 Q_0, where Q_0 was derived from the experimental results of Field et al.[18] as 8.3×10^{-17} m^3/s (cf. Yang et al.[72]). The velocity profile at the inlet was assumed to be parabolic. Because the anus of larvae is open to the surrounding fluid, relative pressure at the outlet was set to zero. The radial velocity at the wall was prescribed by the time derivative of Eq.(3.2.1), and no axial velocity was assumed at the wall.

3.2.3 Basic equations and boundary conditions of bacteria–nutrient coupled transport

Bacterial transport can be described by the following equation [27, 69]:

$$\frac{\partial b}{\partial t} + \mathbf{u}\nabla b = D_b \nabla^2 n + \left(\lambda_g \frac{n}{K_M + n} - \lambda_d \right) b \tag{3.2.4}$$

where b is the number density of bacteria, D_b is the diffusion coefficient of bacteria, λ_g is the maximum growth rate of the bacteria, and λ_d is the natural death rate. The growth rate was assumed to be a function of nutrient concentration n, and K_M is the Monod constant, *i.e.*, the half-saturation constant of nutrients.

The concentration of nutrients was described by the following equation [27, 69]:

$$\frac{\partial n}{\partial t} + \mathbf{u}\nabla n = D_n \nabla^2 n + Y_n \frac{n}{K_M + n} b \tag{3.2.5}$$

where D_n is the diffusion coefficient of nutrients and Y_n is the maximum specific uptake rate of bacterial metabolism.

In the study by Jemielita et al.[29], the zebrafish was held in a specimen chamber containing bacteria-free embryo medium. To reproduce the experimental conditions, a constant nutrient concentration of 150 mol/m^3 and zero bacterial concentration were set at the inlet and outlet. No bacterial flux across the wall of intestine was allowed. Nutrient permeability of the wall was set to either zero or 5.3×10^{-7} m/s[60] to investigate two possible conditions: (a) bacteria take up the nutrient, but the host does not, and (b) both the host and bacteria take up the nutrient. Initially, b was set to 10^{12} m^{-3} around the inlet, *i.e.*, z $\leq$ 1 µm, and to zero over the rest of the domain. This setting was used to reproduce the experimental conditions of Jemielita et al.[29]. As Figure 3.2 shown, we reverse extended the line of the clusters bacterial growth model(solid line) to 0 h, got the initial bacteria number, then divided by the initial volume of intestine to set the initial bacteria concentration. A constant concentration of 150 mol/m^3 was used as the initial nutrient condition over the whole domain.

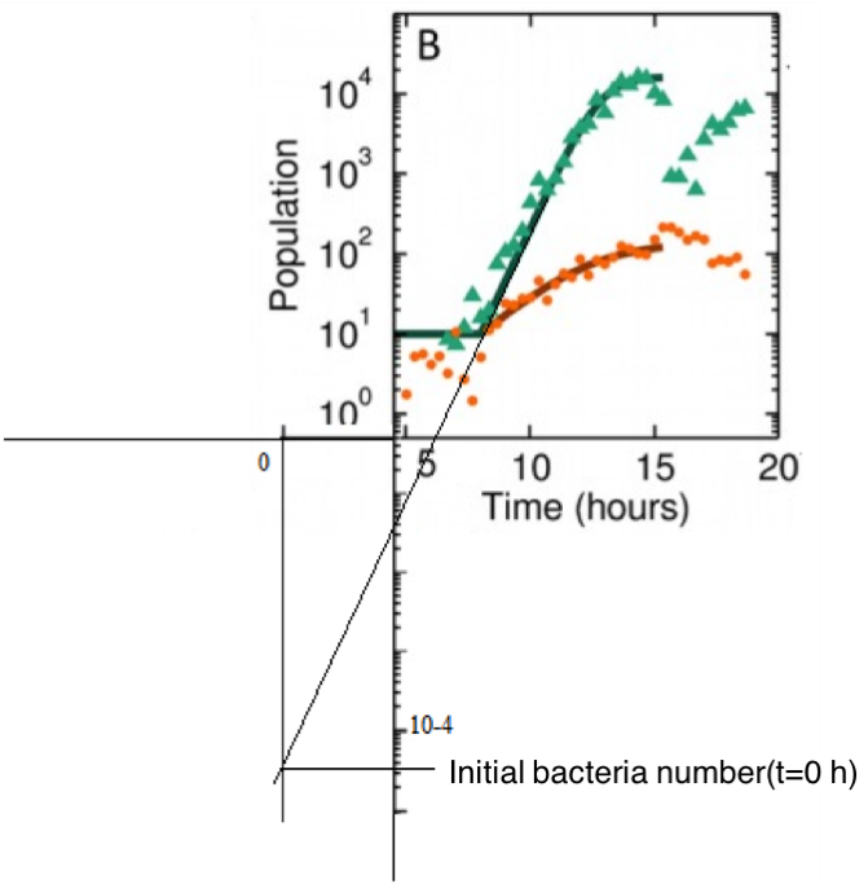

Figure 3.2. Quantification of bacterial load over time for individual bacteria (Orange) and clusters of bacteria (Green)(adapted from [29]). We got the initial bacteria number by reverse extending the line of the clusters of bacterial growth model.

3.2.4 Basic equations and boundary conditions of bacterial transport due to taxis

To understand the biological response of bacteria, taxis was investigated. In the intestine, bacteria may exhibit taxis due to nutrients, pH, temperature, oxygen, antimicrobials, and other factors. To express the nature of taxis mathematically, we introduced a potential field and did not specify the origin of taxis in order to maintain the generality of the model. Bacteria were assumed to exhibit taxis depending on the potential field. The potential field was assumed to have Gaussian profile, and is defined by

$$\varphi = \varphi_{max} \left[-a \left(z - z_0 \right)^2 \right] \tag{3.2.6}$$

where φ_{max} is the maximum value of the potential field. In the experiment by Jemielita et al.[29], *Aeromonas* aggregated around the middle of the intestinal tract. Thus, we set z_0 to be the mid-point of the intestine, *i.e.*, about 700 µm from the inlet. A controls the width of the potential field, and was set to 5.66×10^6 , so that the potential value was φ_{max} /2 at the quarter and three-quarter points of the intestine's length. In order to clarify the effect of the potential form on the spatial heterogeneity of bacterial flora, we also performed calculations with a triangular potential field given by Eq.(3.3.1). The results illustrate that the distribution with the triangular and Gaussian forms are similar not only qualitatively but also quantitatively, and the effect of the functional form is very small. These discussions can be found explicitly in section 3.3.4.

We employed the taxis model of Keller and Segel[32] and expressed bacterial flux due to the potential field as:

$$\mathbf{J} = b \nabla \varphi \tag{3.2.7}$$

where $\mathbf{J}$ is the flux of bacteria, b is the number density of bacteria, and φ is the potential field. The unit of the potential field φ is m^2/s, and $\nabla\varphi$ represents the velocity. This equation indicates that the flux is proportional to the potential gradient. In our investigation of taxis, we assumed that the nutrient concentration was sufficiently high and did not affect the growth rate. Thus, we did not solve the concentration field and assumed that the maximum growth rate of λ_g applied. The

equation governing bacterial transport, in this case, was the following[32, 64]:

$$\frac{\partial b}{\partial t} + (\mathbf{u} + \nabla\varphi)\,\nabla b = D_b \nabla^2 b + \left(\lambda_g - \lambda_d - \nabla^2\varphi\right) b \tag{3.2.8}$$

$$\lambda_g = \begin{cases} 3.2 \times 10^{-4} s^{-1}, & (b \leq 6.5 \times 10^{15} m^{-3}) \\ 0. & (b \geq 6.5 \times 10^{15} m^{-3}) \end{cases} \tag{3.2.9}$$

We set the maximum number density of bacteria to $6.5 \times 10^{15}\mathrm{m}^{-3}$ based on the growth curve obtained by Jemielita et al.[29]. Thus, the growth rate was zero when the local b exceeded $6.5 \times 10^{15}\mathrm{m}^{-3}$(Seen Figure 3.2).

3.2.5 Numerical methods and parameters

The governing equations were solved numerically using the commercial software ANSYS-CFX (ANSYS, USA) with the boundary and initial conditions described. After checking for time step and mesh convergence, the time step was set to 0.025 s for calculations with peristalsis or 10 s for calculations without peristalsis. We checked the bacteria distribution at different locations on the lateral cross-section with compared the time step 1 s and time step 10 s as Figure 3.3. From the results, the maximum relative error is about 0.4%. Thus, we used the time step 10 s for calculation without peristalsis. A structured mesh with 110,580 hexahedral elements and 131,040 nodes was employed. The mesh model was shown as Figure 3.4. We checked the mesh convergence as Figure 2.4 in Chapter 2, not only the velocity distribution, but also the nutrient distribution.

We performed two types of simulations: (a) bacteria–nutrient coupled transport, and (b) bacterial transport with taxis. Bacteria–nutrient coupled transport is described in Section 3.1 using the basic equations and boundary conditions explained in Section 2.3. Bacterial transport with taxis is discussed in Sections 3.1–3.3 using the basic equations and boundary conditions explained in Section 2.4. Peristaltic motion is examined in Section 3.3 using the wall configuration given in Section 2.1. In Sections 3.1 and 3.2, peristaltic motion was neglected, and a long-duration computation was performed. The parameters used in the present study are listed in Table 1. Based on observations by Holmberg et al.[24], Roach et al.[54], Rich et al.[52], and Baker et al.[1], the depth of contraction δ_f was assumed to be 50% of the

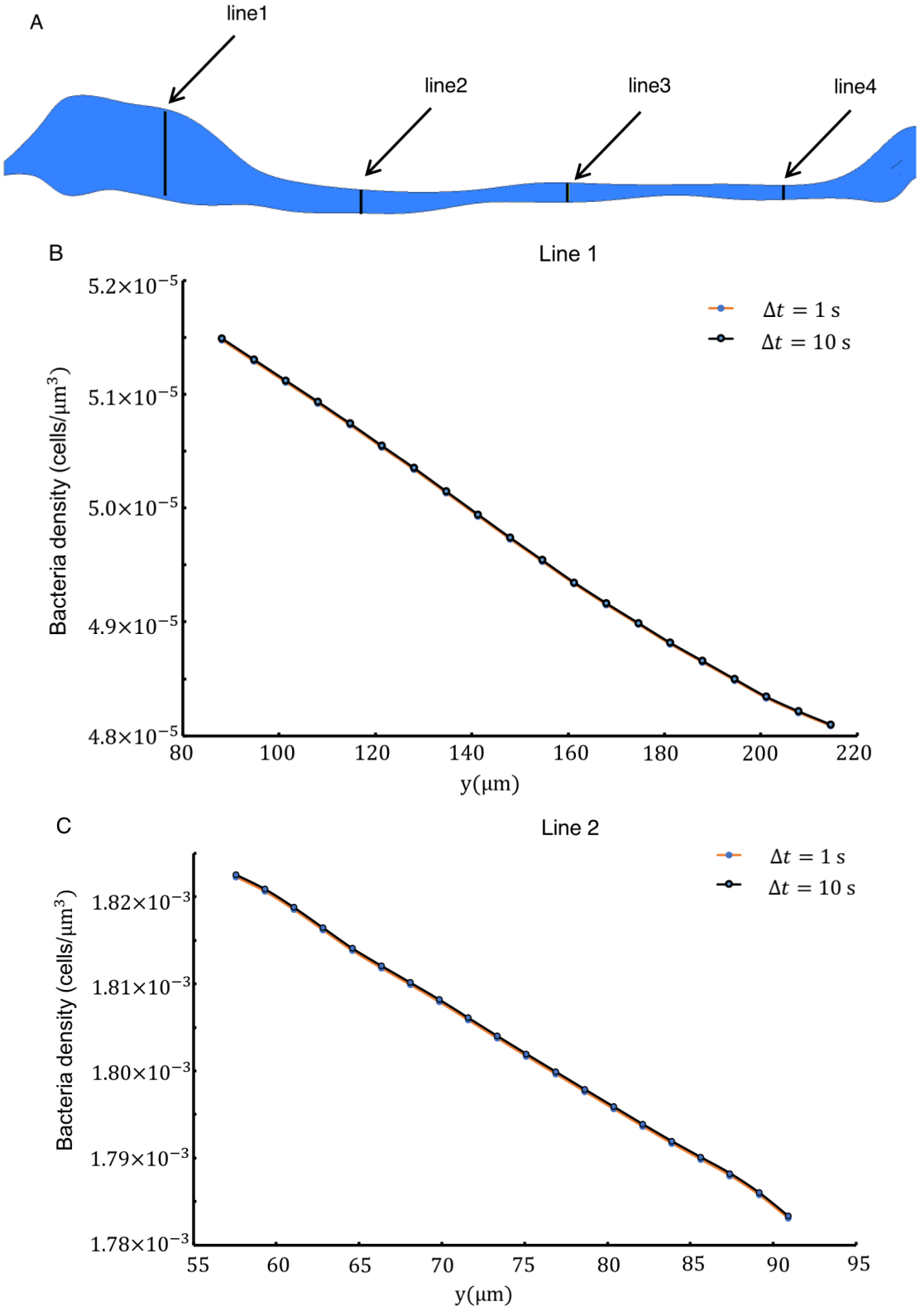
A
line1
line2
line3
line4
B
Line 1
$\Delta t = 1$ s
$\Delta t = 10$ s
Bacteria density (cells/µm^3)
5.2×10^{-5}
5.1×10^{-5}
5.0×10^{-5}
4.9×10^{-5}
4.8×10^{-5}
80
100
120
140
160
180
200
220
y(µm)
C
Line 2
$\Delta t = 1$ s
$\Delta t = 10$ s
Bacteria density (cells/µm^3)
1.82×10^{-3}
1.81×10^{-3}
1.80×10^{-3}
1.79×10^{-3}
1.78×10^{-3}
55
60
65
70
75
80
85
90
95
y(µm)

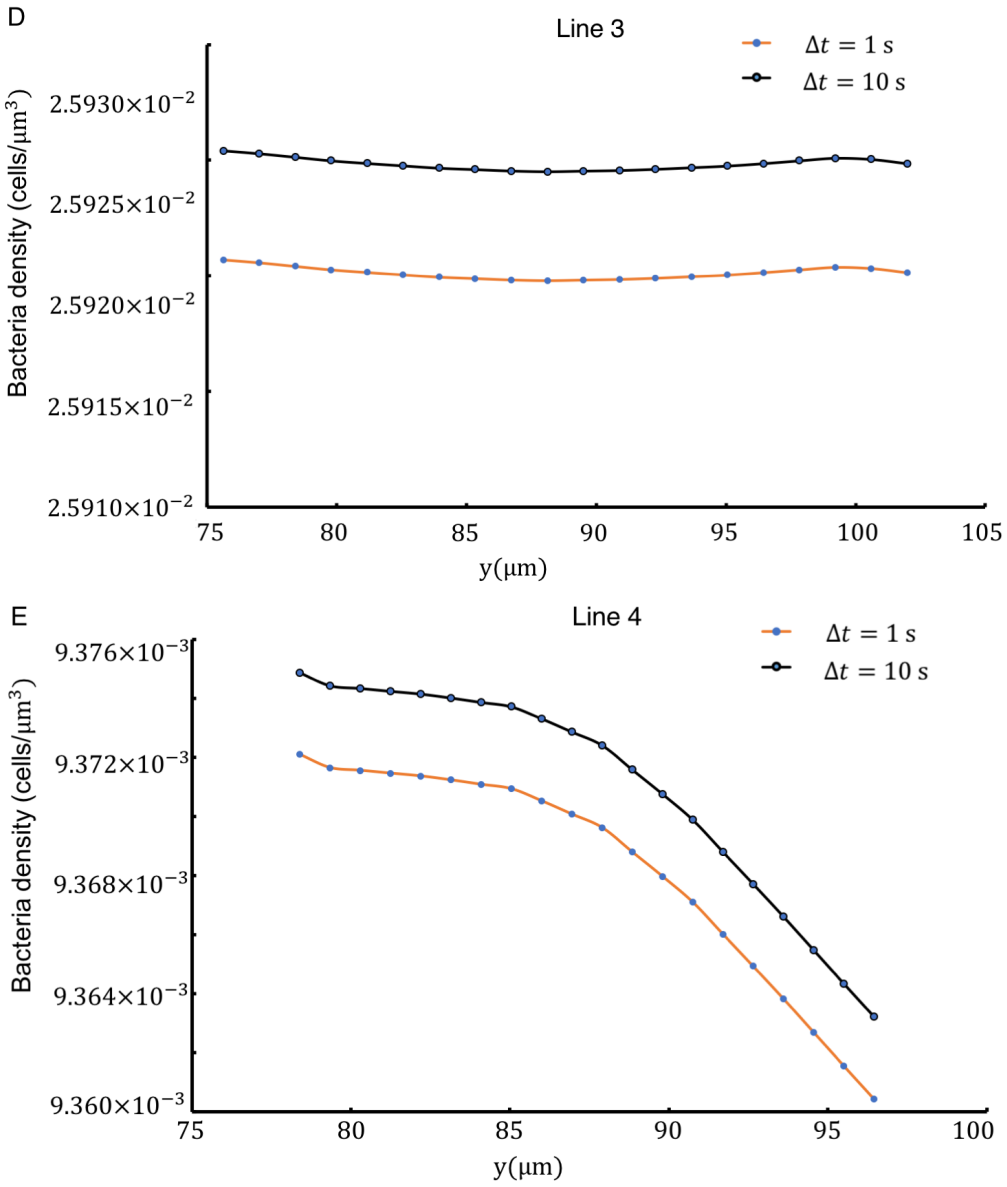

Figure 3.3. The bacteria distribution of results for checking time step. A: the location of selected lines for the time step checking. The lines were on the lateral cross-section.B-D: the bacteria distribution for time step 1 s and time step 10 s at different line.

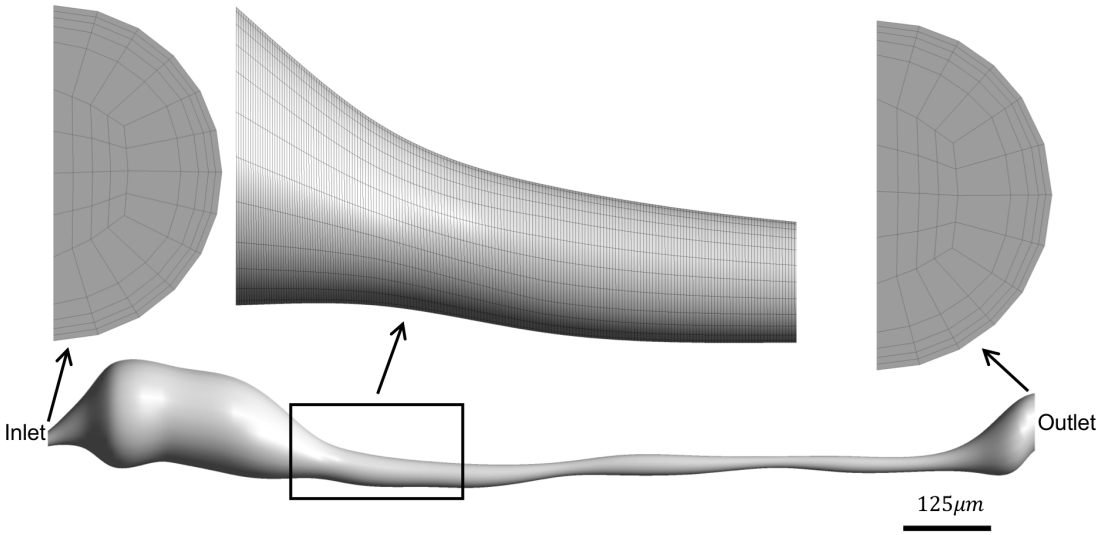

Figure 3.4. A three-dimensionalstructure mesh model of the intestine of a zebrafish larva at 5 days post-fertilization.

radius of the intestine. The propagation velocity of peristalsis (U_c) was assumed to be 15 µm/s. The interval time Δt was assumed to be 24 and 60 s for retrograde and anterograde peristaltic motion, respectively. The travel distance of peristalsis was assumed to be 170 µm for retrograde peristalsis (d_{re}) and 370 µm for anterograde peristalsis (d_{an}). The diffusion coefficient of bacteria was varied over the range D_b = 1 × (10^{-12}–10^{-10}) m^2 /s, and the inlet flow rate was varied over the range Q_{in} = 1–5 Q_0.

3.3 Results

3.3.1 Bacterial distribution based on two hypotheses

In the experiment by Jemielita et al.[29], *Aeromonas* aggregated around the middle of the intestinal tract. We first tried to reproduce this aggregated distribution using the bacteria–nutrient coupled transport hypothesis described in Section 3.3.1. We also investigated the bacterial transport with taxis hypothesis noted in Section 3.3.13.1.2. To quantitatively describe aggregation, we calculated n_c/N, where nc is the number of bacteria in the middle region of the intestine, *i.e.*, from 350 to 1050

Table 3.1. Parameter used in Chapter 3

Parameters for peristaltic motion and geometry		
Depth of peristaltic contraction δ_f	0.5R	R is the radius (R=W/2)
Time interval of peristaltic waves ΔT	ΔT_{re}=24 s ΔT_{an}=60 s	Holmberg et al.[24],Roach et al.[54],Rich et al.[52]
Travel distance of retrograde peristalsis d_{re}	170 µm	Roach et al.[54]
Travel distance of anterograde peristalsis d_{an}	370 µm	Roach et al.[54]
Half width of the peristaltic wave λ_f	$=\delta_f$	Baker et al.[1]
Origin of peristaltic wave generation z_{f0}	550 µm	Determined by comparing with Holmberg et al.[24] and Jemielita et al.[29]
Parameters of bacterial distribution		
Diffusion coefficient of bacteria	$1\times(10^{-12}$ – $10^{-10})\mathrm{m}^2/\mathrm{s}$	
Maximum growth rate in the medium lambda$_g$	3.2×10^{-4} s^{-1}	Calculated from Jemielita et al.[29]
Natural death rate lambda$_d$	1×10^{-5} s^{-1}	Westerwalbesloh et al.[69]
Parameters of nutrient distribution		
Monod constant K_M	4.5 $\mathrm{mol/m}^3$	Westerwalbesloh et al.[69]
Maximum specific uptake of bacterial metabolism	4.7×10^{-16} mol/(cell s)	Westerwalbesloh et al.[69]
Wall permeability to nutrients κ	5.3×10^{-7} m/s	Servais et al.[60]
Diffusion coefficient of glucose	5×10^{-10} m^2/s	Westerwalbesloh et al.[69]
Flow parameters		
Propagation velocity of the peristaltic wave U_c	15 µm/s	Roach et al.[54]
Fluid density ρ	1000 $\mathrm{kg/m}^3$	
Fluid viscosity μ	0.001 Pa·s	
Volume flow rate at the inlet Q_{in}	0 –5 Q_0	Yang et al.[72]

μm, and N is the number of bacteria in the whole intestine. Large n_c/N ratios indicate that bacteria are aggregated in the middle of the intestinal tract. We note that the value of n_c/N in the experiment by Jemielita et al.[29] may be estimated as 0.75 or greater based on the ratio of fluorescence intensities of labeled bacteria.

Bacteria–nutrient coupled transport hypothesis

In this subsection, we used the basic equations and boundary conditions explained in Section 3.2.3. As a boundary condition of nutrients at the wall, two conditions were applied: (a) zero flux, so that bacteria take up nutrients but the host does not, and (b) 5.3×10^{-7} m/s [60], allowing both host and bacteria to take up nutrients.

The results of zero flux conditions in the absence of peristalsis at $t = 10$ h(=36,000 s) are shown in Figure 3.5. Because the wall did not absorb the nutrients, nutrient concentration was large in the whole intestinal tract. Bacteria could grow at almost their maximum growth rate, and the number density of bacteria in-creased to the order of 10^{12}. To discuss bacterial aggregation, we calculated n_c/N and plotted its temporal variability in Figure 3.7. The maximum value of n_c/N over 10h is about 0.14, which is much smaller than the experimental value of 0.75. These results illustrate that the bacteria–nutrient coupled transport hypothesis with zero nutrient flux across the wall is insufficient to explain the bacterial aggregation observed by Jemielita et al.[29].

Next, we examined wall flux of 5.3×10^{-7} m/s rather than zero. The results are shown in Figure 3.6. Since the wall absorbed considerable nutrients, the nutrient concentration was low over the whole intestinal tract. Bacteria could not grow rapidly in this case due to the lack of nutrients. The maximum number density of bacteria was on the order of 10^7. We again calculated n_c/N and plotted its temporal variability in Figure 3.7. We see that the maximum value of n_c/N over 10 h is about 0.14, which is again much smaller than the experimental value of 0.75. The effect of wall flux on n_c/N was small. Hence, the bacteria–nutrient coupled transport hypothesis with nutrient flux to the wall is also insufficient to explain the bacterial aggregation observed in the experiment.

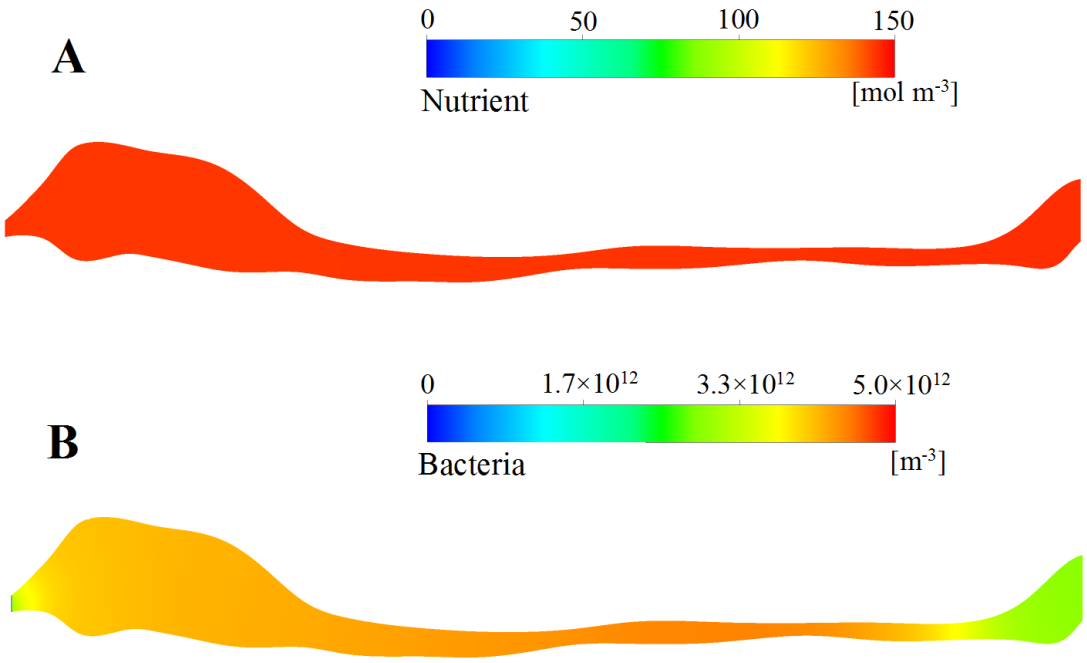

Figure 3.5. Nutrient and bacterial distributions at 10 h with no nutrient flux across the wall and without peristalsis. A: Nutrient distribution. B: Bacterial distribution.

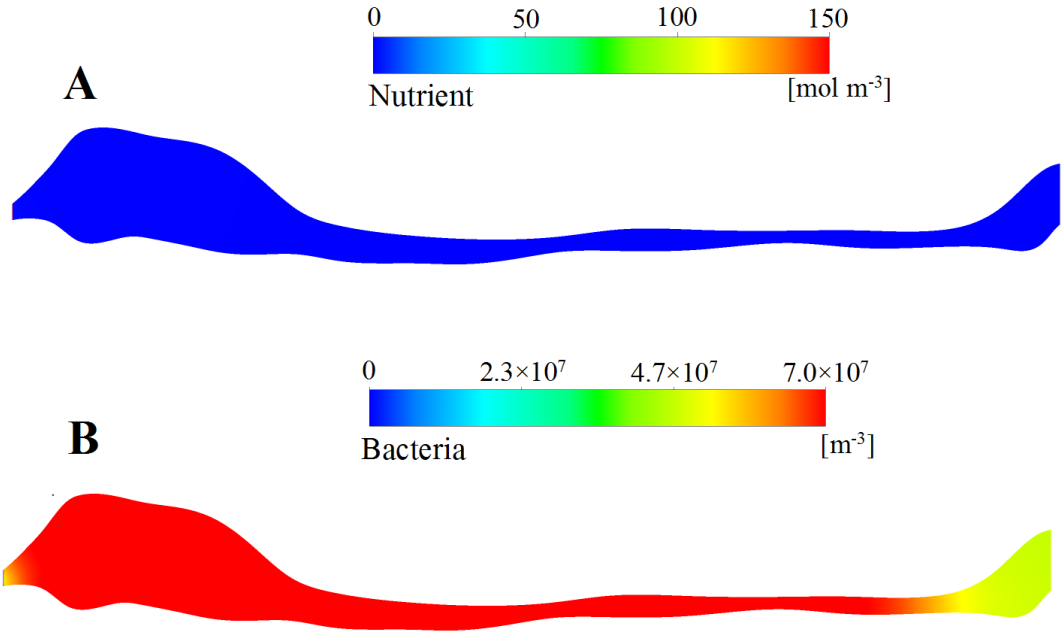

Figure 3.6. Nutrient and bacterial distributions at 10 h under wall flux of 5.3×10^{-7} m/s and without peristalsis. A: Nutrient distribution. B: Bacterial distribution.

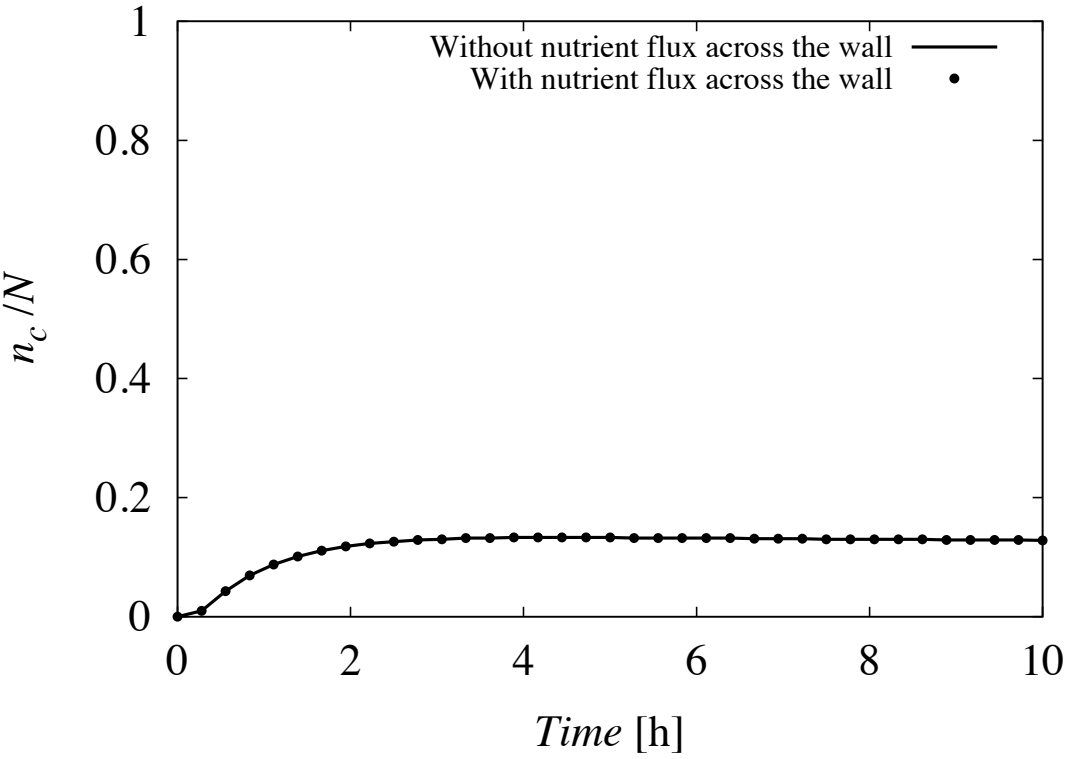

Figure 3.7. Change in the value of n_c/N over time with and without nutrient flux across the wall.

Bacterial transport with taxis hypothesis

In this subsection, we solved the basic equations and boundary conditions explained in Section 3.2.4. To express the taxis of bacteria, a potential field was introduced using Eq.(3.2.6), and its distribution is shown in Figure 3.8A. The potential is high around the middle of the intestinal tract, where bacteria tend to aggregate. Bacterial distributions with various φ_{max} conditions are shown in Figure 3.8B–D. With increasing φ_{max}, bacteria tended to aggregate more strongly. The center of bacterial aggregation was slightly downstream of the geometric center of the intestine, where the potential is greatest. This offset occurs because there was a background bulk flow to- ward the anal outlet, and the bacterial distribution was advected by this background flow. Bacteria did not aggregate too strongly due to their self-diffusivity.

Figure 3.9 shows the change in n_c/N over time under various φ_{max} conditions. The maximum value of n_c/N increased as φ_{max} increased, and n_c/N became greater than 0.75 when $\varphi_{max} = 1.0 \times 10^{-10}$ m^2/s. Thus, the bacterial transport with taxis hypothesis with sufficiently large φ_{max} can reproduce the bacterial aggregation observed in the experiment by Jemielita et al.[29]. Since including taxis was necessary to recreate the bacterial aggregation observed in the experiment, we used the bacterial transport with taxis hypothesis in the following sections.

3.3.2 Effect of bacterial diffusivity D_b and inlet flow rate Q_{in}

As seen in Figure 3.9, n_c/N provides a good measure of bacterial aggregation. The maximum value of n_c/N varied with φ_{max}, as shown in Figure 3.10. We defined φ_0, at which the maximum value of n_c/N becomes 0.75, indicating the potential intensity necessary for generating sufficiently strong bacterial aggregation.

Figure 3.11A shows the effect of the inflow rate Q_{in} on φ_0 with a bacterial diffusivity of $D_b = 1 \times 10^{-11}$ m^2/s. As Q_{in} was increased, the background bulk flow was strengthened. Thus, bacteria tended to flow downstream with increasing Q_{in}. To overcome the bulk flow, bacteria needed to swim fast, which required a large potential field. Thus, in a large-Q_{in} regime, *i.e.*, $Q_{in} > 0.5\ Q_0$, φ_0 increases significantly. When Q_{in} was smaller than $0.3\ Q_0$, however, φ_0 was unaffected by Q_{in}. The reason for this difference is discussed in Section 4.

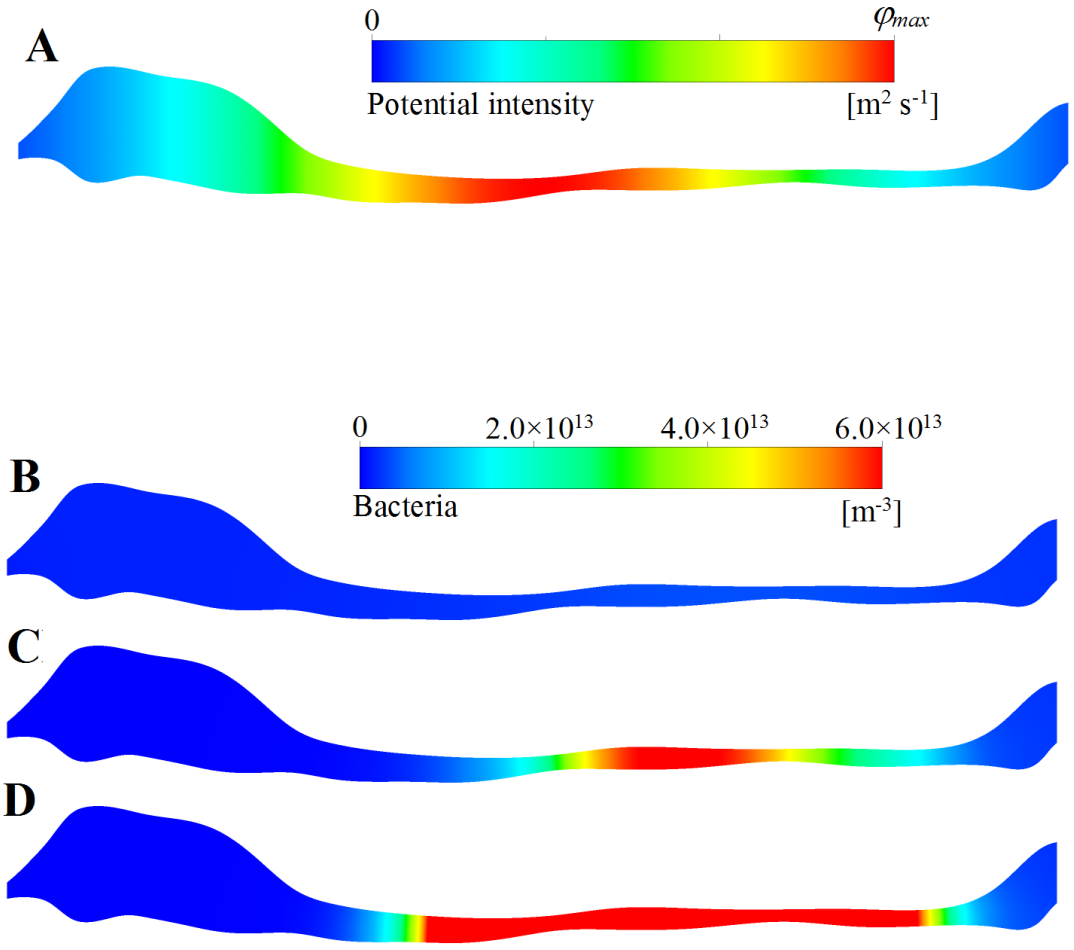

Figure 3.8. Potential field and bacterial distribution at $t = 10$ h under various φ_{max} conditions. A: Potential field described by Eq.(3.2.6). B: Bacterial distribution with $\varphi_{max} = 1.0 \times 10^{-11}$ m^2/s. C: Bacterial distribution with $\varphi_{max} = 5.0 \times 10^{-11}$ m^2/s. D: Bacterial distribution with $\varphi_{max} = 1.0 \times 10^{-10}$ m^2/s.

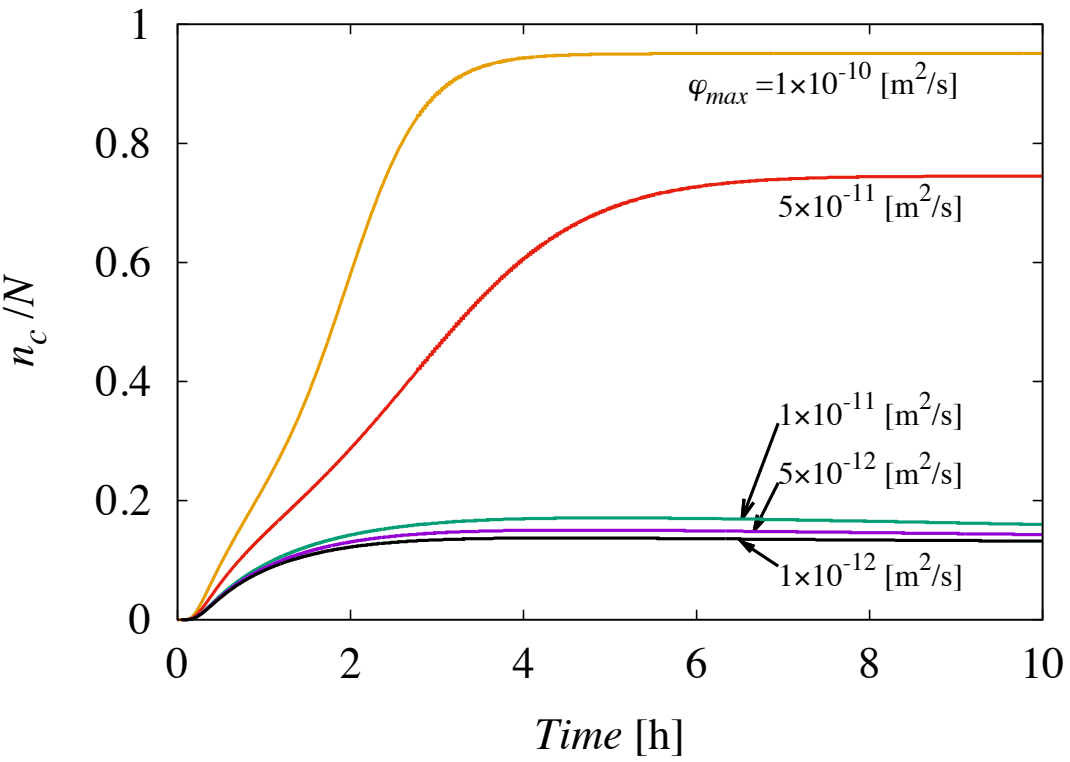

Figure 3.9. Change in the value of n_c/N over time with various maximum potential intensity (φ_{max}) conditions.

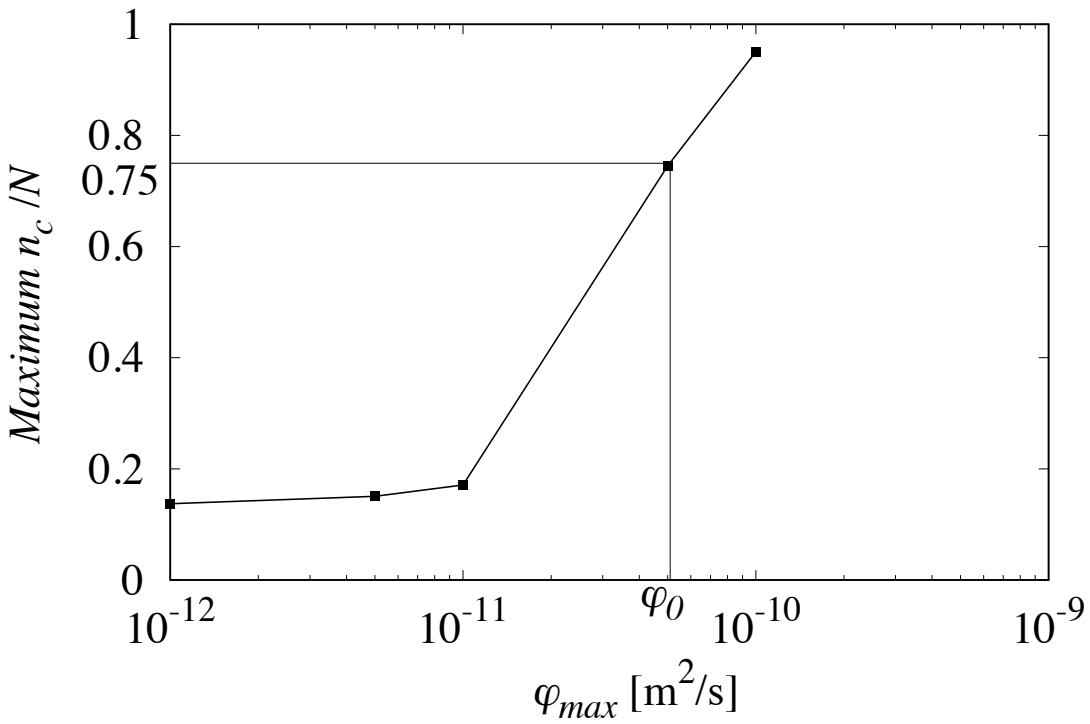

Figure 3.10. Maximum value of n_c/N during $t = 0$ –10 h under various φ_{max} conditions. φ_0 is defined as the value at which the maximum n_c/N reaches 0.75.

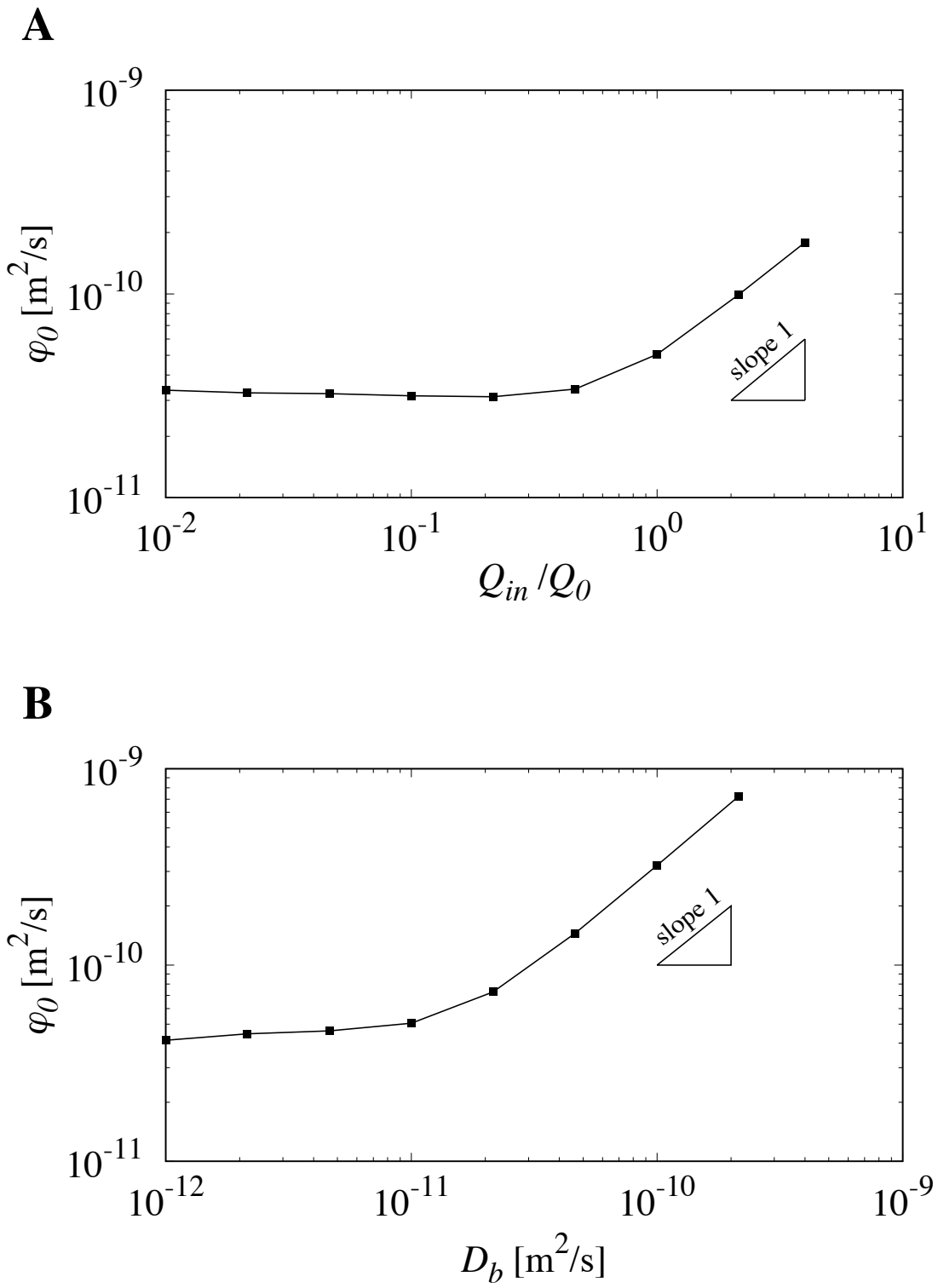

Figure 3.11. Effects of major parameters on the aggregative coefficientφ_0. A: Effect of $Q_{in}(D_b = 1 \times 10^{-11}$ m^2/s). B: Effect of D_b ($Q_{in} = Q_0$).

Figure 3.11B shows the effect of the bacterial diffusion coefficient Db on φ_0 under the condition of $Q_{in} = Q_0$. When D_b is larger than 3×10^{-11} m^2/s, φ_0 increases almost linearly with D_b. On the other hand, when D_b is smaller than 1×10^{-11} m^2/s, φ_0 is unaffected by D_b. The cause of this pattern will also be detailed in Section 3.4.

3.3.3 Effect of peristalsis

We investigated the effect of peristalsis on bacterial aggregative taxis. Figure 3.12 shows the pressure distribution and velocity vectors around the narrowings associated with retrograde and anterograde peristalses. We noted that a pressure difference was generated at the narrowings of the retrograde and anterograde peristalses and a large velocity was generated around these narrowings.

The changes in the positions of 300 tracer particles during peristalsis over 120s is shown in Figure 3.13. The tracer particles were displaced considerably, which induced mixing in the intestine, as discussed in Yang et al.[72]. Thus, peristalsis had the effect of increasing the diffusivity of bacteria in the intestine.

Because computation of peristaltic motion required a long time, the bacterial transport simulation without peristaltic motion was first solved for 7 h, which is sufficient to obtain a converged value of n_c/N. Then, this result was set as the initial condition for peristaltic simulation and calculated for about 30 min based on the results of Yang et al.[72], which was sufficient to describe the mixing function of the zebrafish intestine. Next, the time averaged n_c/N was calculated for the last 2 min, and then we evaluated φ_0 when the time average of n_c/N reaches 0.75. The results of φ_0 during peristaltic motion under various Q_{in} and D_b conditions are shown in Figure 3.14. The value of φ_0 increased when peristaltic motion was considered. Since the comparison in Figure 3.14 was made under the same flow rate condition, the increase in φ_0 was likely caused by the increase in the mixing due to the peristalsis. When there is a peristaltic motion, therefore, stronger taxis is necessary to induce bacterial aggregation.

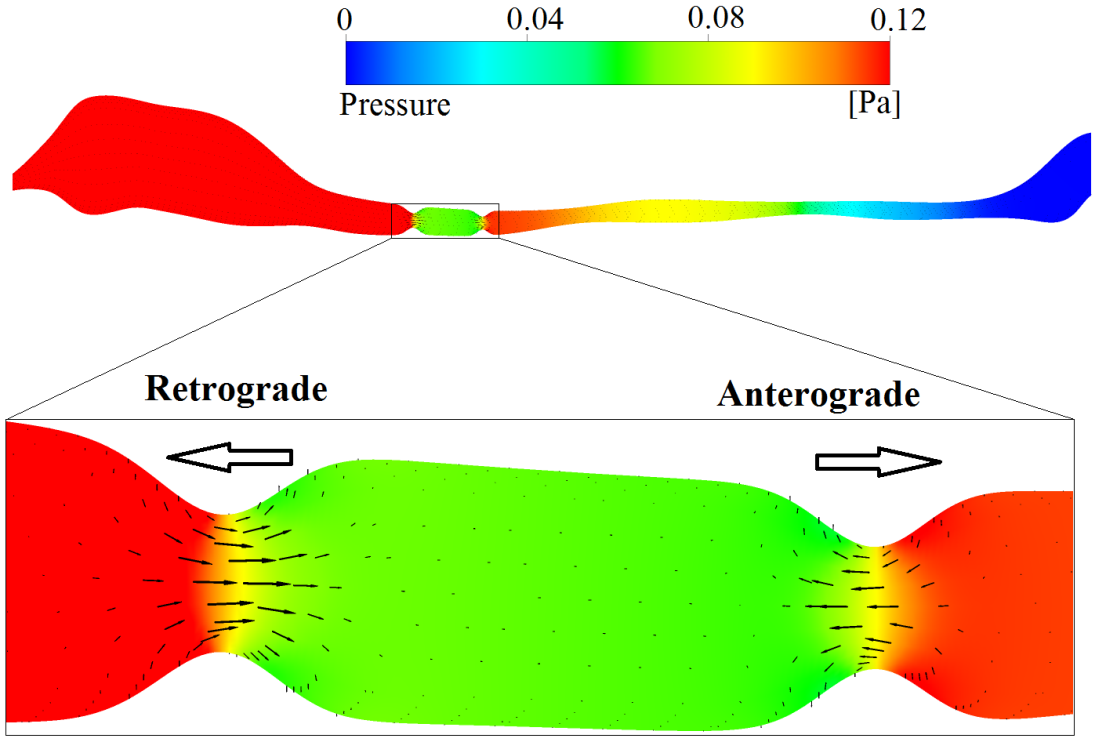

Figure 3.12. Pressure distribution and velocity vectors at 5 s. The large white arrows indicate the directions of retrograde and anterograde peristalses.

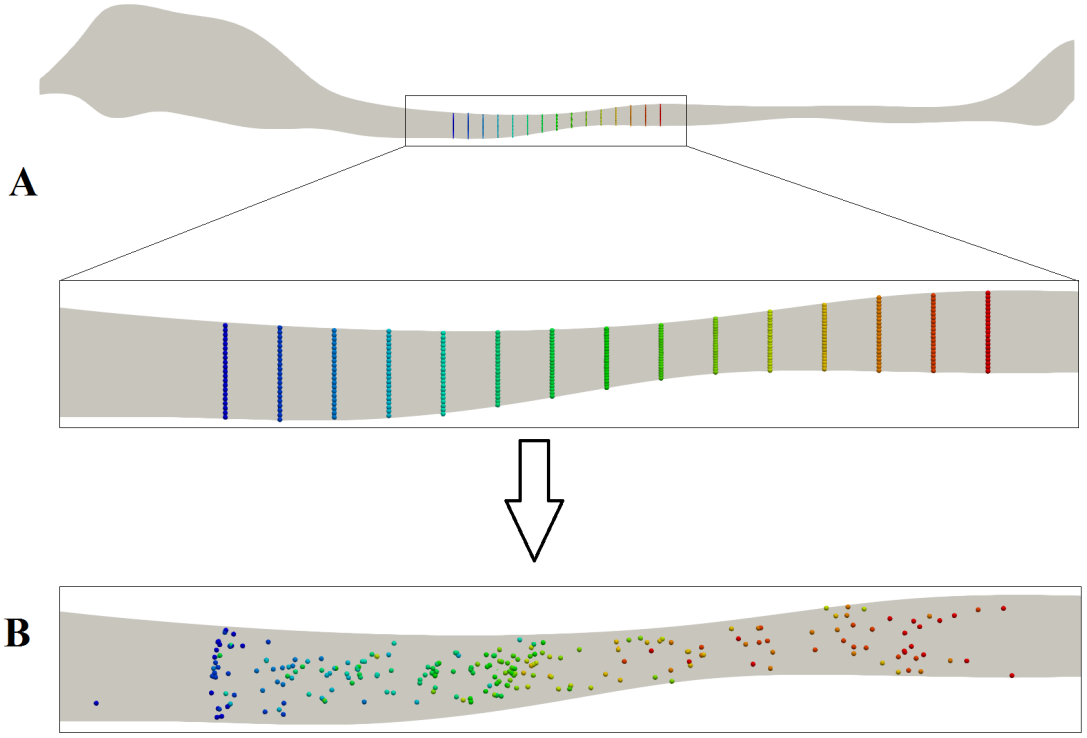

Figure 3.13. Changes in the positions of 300 tracer particles, initially placed perpendicular to the z-axis, due to peristalsis over 120 s. A: Initial position of particles. B: Final position of particles after 120 s.

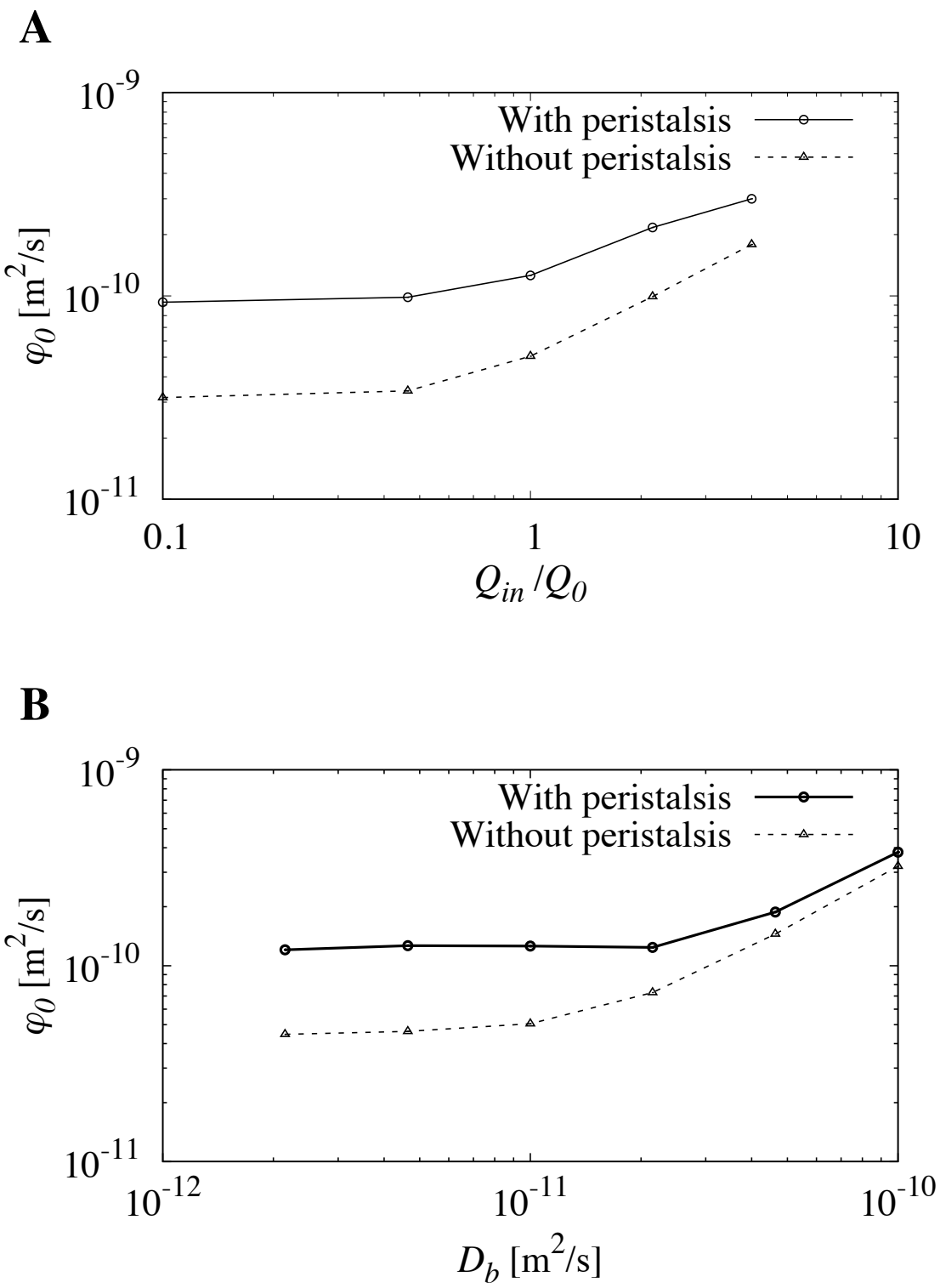

Figure 3.14. φ_0 with and without peristaltic motion under various Q_{in} and D_b conditions. A: Effect of $Q_{in}(D_b = 1 \times 10^{-11}$ m^2/s). B: Effect of D_b ($Q_{in} = Q_0$).

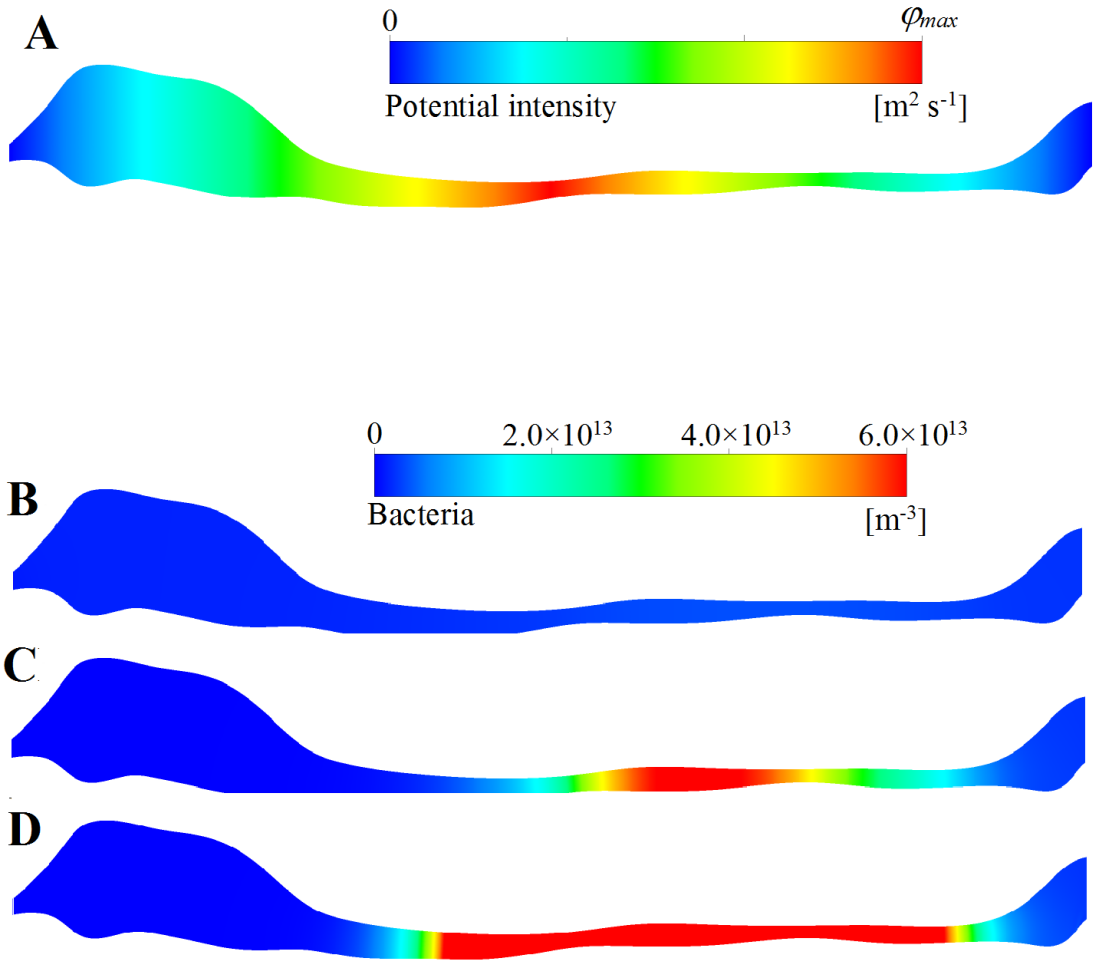

Figure 3.15. Potential field and bacterial distribution obtained by the triangular potential form given by Eq.(3.3.1) at $t = 10$ h. A: Potential field described by Eq.(3.3.1). B: Bacterial distribution with $\varphi_{max} = 1.0\times10^{-11}$ m^2/s. C: Bacterial distribution with $\varphi_{max} = 5.0\times10^{-11}$ m^2/s. D: Bacterial distribution with $\varphi_{max} = 1.0\times10^{-10}$ m^2/s.

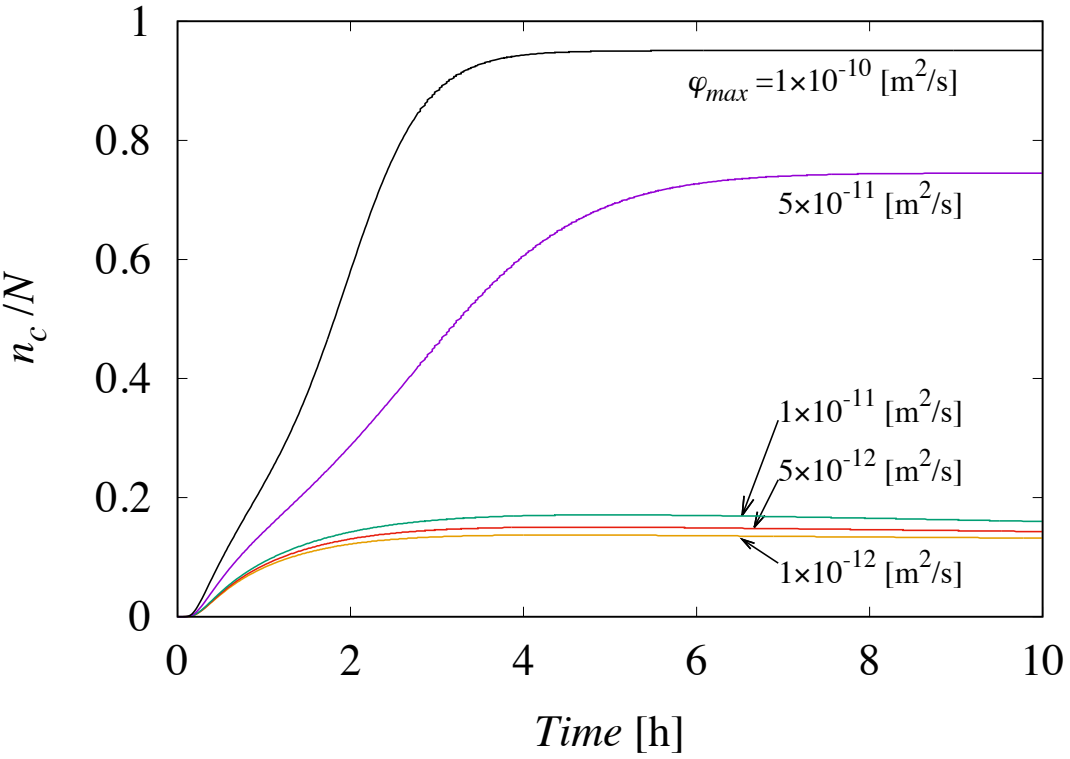

Figure 3.16. Change in the value of n_c/N over time obtained by the triangular potential form given by Eq.(3.3.1)

3.3.4 Effect of potential form

In order to clarify the effect of the potential form on the spatial heterogeneity of bacterial flora, we performed additional calculations with a triangular potential field given by

$$\varphi = \varphi_{max} \frac{2}{L} \left(\frac{L}{2} - |z - z_0| \right) \tag{3.3.1}$$

where φ_{max} is the maximum value of the potential field. z_0 was set to be the midpoint of the intestine, *i.e.*, about 700 µm from the inlet. L is the intestine's length. The triangular potential field is employed here, because it is one of the simplest functional forms and the form is considerably different from the Gaussian form. The obtained results are shown in Figures 3.15 and 3.16. We see that the distribution with the triangular and Gaussian forms are similar not only qualitatively but also quantitatively, and the effect of the functional form is very small.

3.4 Discussion

To understand the results described in Section 3.3, we used a scaling argument in this section. Bacteria showed taxis, and the tendency of this taxis was described by Eq.(3.2.7). The taxis velocity of bacteria U_φ can be scaled as the gradient of the potential in the longitudinal direction, *i.e.*, $U_\varphi \sim \varphi_0/\mathrm{L}$, where L is the half-length of the intestinal tract. There are two kinds of velocities that prevent bacterial aggregation; (a) velocity generated by the background bulk flow U_Q, and (b) velocity generated by the diffusion of bacteria U_D. U_Q can be scaled simply as the average velocity at the center of the intestinal tract, where bacterial aggregation was observed experimentally, *i.e.*, $U_Q \sim \mathrm{Q}_{in} / A_m$, where A_m is the cross-section area in the middle of the intestine, z_0. U_D may be scaled as $U_D \sim \mathrm{D}_b/\mathrm{L}$, given that velocity increases with the diffusion constant, but decreases with distance. To achieve bacterial aggregation, the taxis velocity of bacteria U_φ must be larger than sum of the velocities U_Q and U_D . Hence, the condition $U_\varphi > U_Q + U_D$ must be satisfied to achieve bacterial aggregation.

To determine whether the proposed scaling was satisfied in the present results, we re-plotted the results of Figure 3.11 with U_φ, U_Q, and U_D as axes, as shown in Figure 3.17. In Figure 3.17, the two upper curves with large circles indicate U_φ obtained from the parametric study shown in Figure 3.11. The two middle lines are

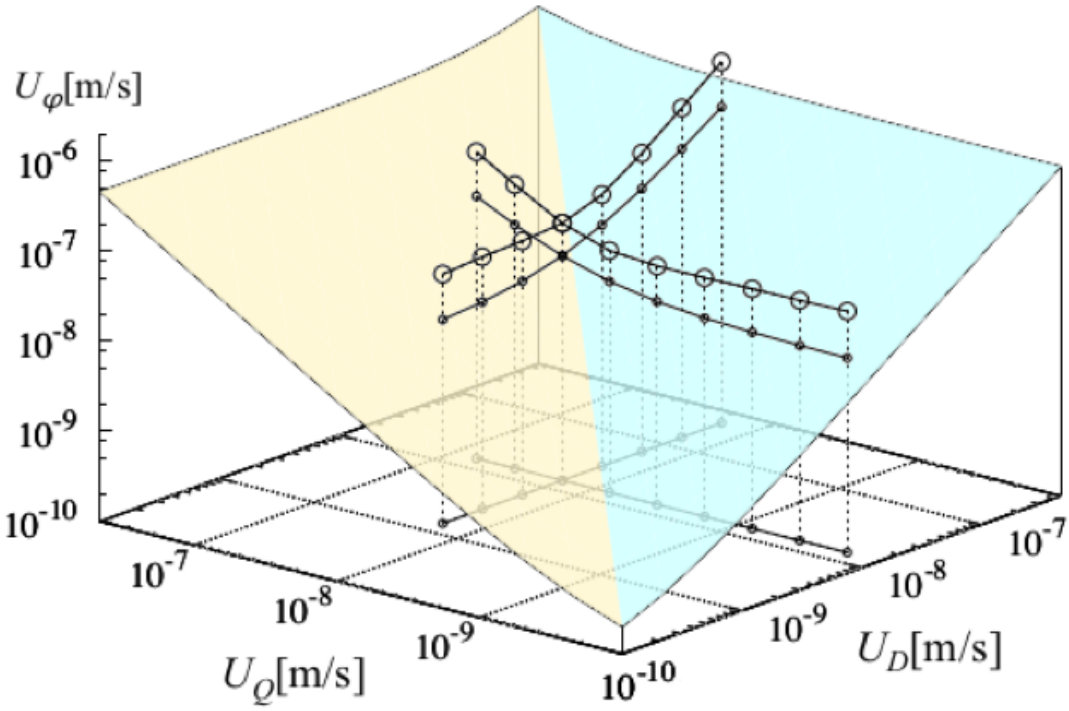

Figure 3.17. Re-plot of the results shown in Figure 3.11 with U_φ, U_Q, and U_D as axes. The two upper curves with large circles are U_φ, and the two middle lines are projections of U_φ on the yellow and blue curved faces that represent the surfaces of $(U_Q + U_D)$.

projections of U_φ on the yellow and blue curved faces, indicating the surfaces of (U_Q $+U_D$). The U_φ curves exist above the surfaces of ($U_Q + U_D$). We therefore conclude that the taxis velocity of bacteria U_φ must be larger than the sum of velocities U_Q and U_D to achieve bacterial aggregation.

Figure 3.17 also indicates the reason why φ_0 was not strongly affected by Q_{in} in the low-Q_{in} regime in Figure 3.11A. The low-Q_{in} regime in Figure 3.11A correspond to low-U_Q in Figure 12, where the blue curved faces exists. Although U_Q decreased linearly with Q_{in}, U_D was unaffected by Q_{in} and had a constant value of D_b/L greater than U_Q. Thus, the value of (U_Q $+U_D$) was approximately constant in the low-Q_{in} regime, explaining why φ_0 was not strongly affected by Q_{in} in the low-Q_{in} regime in Figure 8A. Similarly, the reason that φ_0 was unaffected by D_b in the low-D_b regime in Figure 3.11B may be associated with the constant value of U_Q $= Q_{in}/A_m$ in the low-D_b regime.

Moreover, the φ_0 may have increased when peristalsis was introduced in Figure 3.14 due to the increase of U_D. Without peristalsis, U_D is scaled as U_D $\sim$D$_b$/L, where D_b is the diffusion coefficient of bacteria. By introducing peristaltic motion, bacteria are strongly mixed in the flow generated by the peristalsis, which has the ef- fect of increasing the effective diffusivity of bacteria. Thus, effective U_D also increased due to peristaltic motion, and the value of φ_0 0 increased, as shown in Figure 3.14. We believe that these scaling arguments are useful for understanding bacterial aggregation due to taxis under various conditions.

3.5 Summary

We developed a computational model to describe the heterogeneous distribution of bacteria in the intestine of zebrafish larvae. We examined two hypotheses; (a) the bacteria–nutrient coupled transport hypothesis, and (b) the bacterial transport with taxis hypothesis. The results showed that the bacterial aggregation observed by Jemielita et al.[29] could be reproduced under the bacterial transport with taxis hypothesis with sufficiently large φ_{max}. Using the bacterial transport with taxis hypothesis, we investigated the potential intensity φ_0 at which the maximum value of n_c/N reaches 0.75. In high-Q_{in} or D_b regimes, φ_0 increased nearly linearly with

Q_{in} or D_b. In low-Q_{in} or D_b regimes, on the other hand, φ_0 was unaffected by Q_{in} or D_b. Peristaltic motion in the intestine increased φ_0 . These tendencies were well explained by scaling arguments, which showed that the taxis velocity of bacteria U must be larger than the sum of velocities U_Q and U_D,*i.e.*,$U_\varphi > U_Q + U_D$.The results of our model will be useful for a greater understanding of microbial flora in the intestine.

Chapter 4

Conclusion

In this study, we proposed an anatomically realistic three-dimensional geometric model of the zebrafish larval intestine to investigate the transport phenomena and bacterial aggregation phenomena by numerical simulation method.

First, we investigated the transport phenomena caused by peristaltic motion in the intestine of zebrafish larvae by numerical simulation in Chapter 2. There are two kinds of the peristaltic motion in the intestine of zebrafish. One is retrograde peristaltic motion, which was major contributor to the mixing function. Based on the results in this thesis, the dispersion caused by retrograde peristalsis over 30 min was in the order of 10^{-12} m^2/s, which is greater than the Brownian diffusion of a sphere of 0.4 µm diameter. Another is anterograde peristaltic motion which contributed mainly to the pumping function. And this function induced a pressure decrease in the order of millipasacals, which may reduce the activation and maintenance heat of intestinal muscle.

Then, we developed a computational model to describe the heterogeneous distribution of bacteria in the intestine of zebrafish larvae in Chapter 3. We examined the bacteria–nutrient coupled transport hypothesis, and the bacterial transport with taxis hypothesis. From the results in this thesis, the bacterial aggregation phenomena observed by Jemielita et al.[29] could be reproduced under the bacterial transport with taxis hypothesis with sufficiently large φ_{max}. Using the bacterial transport with taxis hypothesis, we investigated the potential intensity φ_0 at which the maximum value of n_c/N reaches 0.75. In high-Q_{in} or D_b regimes, φ_0 increased nearly linearly with Q_{in} or D_b. In low-Q_{in} or D_b regimes, on the other hand, φ_0 was unaffected by Q_{in} or D_b. Due to the mixing function, the peristaltic motion in the intestine

increased φ_0 . These tendencies were well explained by scaling arguments, which showed that the taxis velocity of bacteria U_φ must be larger than the sum of velocities U_Q and U_D, *i.e.*, $U_\varphi > U_Q + U_D$.

These findings in this thesis will be useful for a greater understanding of the mixing and pumping functions of the intestine of zebrafish larvae, and enhance our understanding of microbial flora in the intestine.

References

[1] R Baker, M Taormina, M Jemielita, and R Parthasarathy. (2015) A combined light sheet fluorescence and differential interference contrast microscope for live imaging of multicellular specimens. *Journal of Microscopy* **258**, 105–112.

[2] JM Bates, J Akerlund, E Mittge, and K Guillemin. (2007) Intestinal Alkaline Phosphatase Detoxifies Lipopolysaccharide and Prevents Inflammation in Zebrafish in Response to the Gut Microbiota. *Cell Host & Microbe* **2**, 371–382.

[3] JM Bates, E Mittge, J Kuhlman, KN Baden, SE Cheesman, and K Guillemin. (2006) Distinct signals from the microbiota promote different aspects of zebrafish gut differentiation. *Developmental Biology* **297**, 374–386.

[4] JP Briggs. (2002) The zebrafish: a new model organism for integrative physiology. *American Journal of Physiology - Regulatory, Integrative and Comparative Physiology* **282**, R3–R9.

[5] S Brugman. (2016) The zebrafish as a model to study intestinal inflammation. *Developmental & Comparative Immunology* **64**, 82–92.

[6] GO Canny and BA McCormick. (2008) Bacteria in the Intestine, Helpful Residents or Enemies from Within? *Infection and Immunity* **76**, 3360–3373.

[7] I Cho and MJ Blaser. (2012) The human microbiome: at the interface of health and disease. *Nature Reviews Genetics* **13**, 260–270.

[8] JL Cocchiaro and JF Rawls. (2013) Microgavage of Zebrafish Larvae. *Journal of Visualized Experiments*.

[9] J Cremer, I Segota, Cy Yang, M Arnoldini, JT Sauls, Z Zhang, E Gutierrez, A Groisman, and T Hwa. (2016) Effect of flow and peristaltic mixing on bacterial growth in a gut-like channel. *Proceedings of the National Academy of Sciences* **113**, 11414–11419.

[10] C Crosnier. (2005) Delta-Notch signalling controls commitment to a secretory fate in the zebrafish intestine. *Development* **132**, 1093–1104.

[11] EF DeLong. (2014) Alien Invasions and Gut "Island Biogeography". *Cell* **159**, 233–235.

[12] L Dethlefsen, M McFall-Ngai, and DA Relman. (2007) An ecological and evolutionary perspective on human–microbe mutualism and disease. *Nature* **449**, 811–818.

[13] GP Donaldson, SM Lee, and SK Mazmanian. (2015) Gut biogeography of the bacterial microbiota. *Nature Reviews Microbiology* **14**, 20–32.

[14] K Dooley. (2000) Zebrafish: a model system for the study of human disease. *Current Opinion in Genetics & Development* **10**, 252–256.

[15] K Drescher, J Dunkel, LH Cisneros, S Ganguly, and RE Goldstein. (2011) Fluid dynamics and noise in bacterial cell-cell and cell-surface scattering. *Proceedings of the National Academy of Sciences of the United States of America* **108**, 10940–10945.

[16] W DRIEVER, DEREK STEMPLE, AI.KXANDI SCHIER, and SOLNICA KREZEL. (1994) Zebrafish:genetic tools for studyingvertebrate development. *Trends in Genetics* **10**, 152–159.

[17] RJ Egan, CL Bergner, PC Hart, JM Cachat, PR Canavello, MF Elegante, SI Elkhayat, BK Bartels, AK Tien, DH Tien, S Mohnot, E Beeson, E Glasgow, H Amri, Z Zukowska, and AV Kalueff. (2009) Understanding behavioral and physiological phenotypes of stress and anxiety in zebrafish. *Behavioural Brain Research* **205**, 38–44.

[18] HA Field, KA Kelley, L Martell, AM Goldstein, and FC Serluca. (2009) Analysis of gastrointestinal physiology using a novel intestinal transit assay in zebrafish. *Neurogastroenterology & Motility* **21**, 304–312.

[19] HA Field, PDS Dong, D Beis, and DYR Stainier. (2003) Formation of the digestive system in zebrafish. II. Pancreas morphogenesis. *Developmental Biology* **261**, 197–208.

[20] HA Field, EA Ober, T Roeser, and DY Stainier. (2003) Formation of the digestive system in zebrafish. I. Liver morphogenesis. *Developmental biology* **253**, 279–290.

[21] HJ Flint, SH Duncan, KP Scott, and P Louis. (2007) Interactions and competition within the microbial community of the human colon: links between diet and health. *Environmental Microbiology* **9**, 1101–1111.

[22] HJ Flint, KP Scott, P Louis, and SH Duncan. (2012) The role of the gut microbiota in nutrition and health. *Nature Reviews Gastroenterology & Hepatology* **9**, 577–589.

[23] A Holmberg. (2004) Ontogeny of the gut motility control system in zebrafish Danio rerio embryos and larvae. *Journal of Experimental Biology* **207**, 4085–4094.

[24] A Holmberg, C Olsson, and GW Hennig. (2007) TTX-sensitive and TTX-insensitive control of spontaneous gut motility in the developing zebrafish (Danio rerio) larvae. *Journal of Experimental Biology* **210**, 1084–1091.

[25] E Homsher, WFHM Mommaerts, NV Ricchiuti, and A Wallner. (1972) Activation heat, activation metabolism and tension-related heat in frog semitendinosus muscles. *The Journal of Physiology* **220**, 601–625.

[26] K Howe et al. (2013) The zebrafish reference genome sequence and its relationship to the human genome. *Nature* **496**, 498–503.

[27] T Ishikawa, T Sato, G Mohit, Y Imai, and T Yamaguchi. (2011) Transport phenomena of microbial flora in the small intestine with peristalsis. *Journal of Theoretical Biology* **279**, 63–73.

[28] T Ishikawa and TJ Pedley. (2007) Diffusion of swimming model microorganisms in a semi-dilute suspension. *Journal of Fluid Mechanics* **588**, 437–462.

[29] M Jemielita, MJ Taormina, AR Burns, JS Hampton, AS Rolig, K Guillemin, and R Parthasarathy. (2014) Spatial and Temporal Features of the Growth of a Bacterial Species Colonizing the Zebrafish Gut. *mBio* **5**, e01751–14.

[30] AV Kalueff, AM Stewart, and R Gerlai. (2014) Zebrafish as an emerging model for studying complex brain disorders. *Trends in Pharmacological Sciences* **35**, 63–75.

[31] N Kamada, SU Seo, GY Chen, and G Núñez. (2013) Role of the gut microbiota in immunity and inflammatory disease. *Nature Reviews Immunology* **13**, 321–335.

[32] EF Keller and LA Segel. (1971) Model for chemotaxis. *Journal of theoretical biology* **30**, 225–234.

[33] CC Lan and DR Love. (2012) Molecular Characterisation of Bacterial Community Structure along the Intestinal Tract of Zebrafish (*Danio rerio*): A Pilot Study. *ISRN Microbiology* **2012**, 1–10.

[34] ST Laughlin, JM Baskin, SL Amacher, and CR Bertozzi. (2008) In Vivo Imaging of Membrane-Associated Glycans in Developing Zebrafish. *Science* **320**, 664–667.

[35] EE LeClair and J Topczewski. (2010) Development and Regeneration of the Zebrafish Maxillary Barbel: A Novel Study System for Vertebrate Tissue Growth and Repair. *PLoS ONE* **5**, e8737.

[36] SM Lee, GP Donaldson, Z Mikulski, S Boyajian, K Ley, and SK Mazmanian. (2013) Bacterial colonization factors control specificity and stability of the gut microbiota. *Nature* **501**, 426–429.

[37] WJ Lee and K Hase. (2014) Gut microbiota–generated metabolites in animal health and disease. *Nature Chemical Biology* **10**, 416–424.

[38] GJ Lieschke and PD Currie. (2007) Animal models of human disease: zebrafish swim into view. *Nature Reviews Genetics* **8**, 353–367.

[39] BA Link and RF Collery. (2015) Zebrafish Models of Retinal Disease. *Annual Review of Vision Science* **1**, 125–153.

[40] CA MacRae and RT Peterson. (2015) Zebrafish as tools for drug discovery. *Nature Reviews Drug Discovery* **14**, 721–731.

[41] C Maximino, TM de Brito, AW da Silva Batista, AM Herculano, S Morato, and A Gouveia. (2010) Measuring anxiety in zebrafish: A critical review. *Behavioural Brain Research* **214**, 157–171.

[42] AL Menke, JM Spitsbergen, APM Wolterbeek, and RA Woutersen. (2011) Normal Anatomy and Histology of the Adult Zebrafish. *Toxicologic Pathology* **39**, 759–775.

[43] AN Ng, TA de Jong-Curtain, DJ Mawdsley, SJ White, J Shin, B Appel, PDS Dong, DY Stainier, and JK Heath. (2005) Formation of the digestive system in zebrafish: III. Intestinal epithelium morphogenesis. *Developmental Biology* **286**, 114–135.

[44] JK Nicholson, E Holmes, J Kinross, R Burcelin, G Gibson, W Jia, and S Pettersson. (2012) Host-Gut Microbiota Metabolic Interactions. *Science* **336**, 1262–1267.

[45] P Niethammer, C Grabher, AT Look, and TJ Mitchison. (2009) A tissue-scale gradient of hydrogen peroxide mediates rapid wound detection in zebrafish. *Nature* **459**, 996–999.

[46] EMM Quigley. (2013) Gut Bacteria in Health and Disease. 10.

[47] J Rall. *Mechanism of Muscular Contraction.*

[48] JA Rall and BA Schottelius. (1973) Energetics of Contraction in Phasic and Tonic Skeletal Muscles of the Chicken. *The Journal of General Physiology* **62**, 303–323.

[49] JF Rawls, MA Mahowald, AL Goodman, CM Trent, and JI Gordon. (2007) In vivo imaging and genetic analysis link bacterial motility and symbiosis in the zebrafish gut. *Proceedings of the National Academy of Sciences* **104**, 7622–7627.

[50] JF Rawls, MA Mahowald, RE Ley, and JI Gordon. (2006) Reciprocal Gut Microbiota Transplants from Zebrafish and Mice to Germ-free Recipients Reveal Host Habitat Selection. *Cell* **127**, 423–433.

[51] O Rendueles, L Ferrières, M Frétaud, E Bégaud, P Herbomel, JP Levraud, and JM Ghigo. (2012) A New Zebrafish Model of Oro-Intestinal Pathogen Colonization Reveals a Key Role for Adhesion in Protection by Probiotic Bacteria. *PLoS Pathogens* **8**, e1002815.

[52] A Rich, S Gordon, C Brown, SJ Gibbons, K Schaefer, G Hennig, and G Farrugia. (2013) Kit Signaling Is Required for Development of Coordinated Motility Patterns in Zebrafish Gastrointestinal Tract. *Zebrafish* **10**, 154–160.

[53] S Rinkwitz, P Mourrain, and TS Becker. (2011) Zebrafish: An integrative system for neurogenomics and neurosciences. *Progress in Neurobiology* **93**, 231–243.

[54] G Roach, R Heath Wallace, A Cameron, R Emrah Ozel, CF Hongay, R Baral, S Andreescu, and KN Wallace. (2013) Loss of ascl1a prevents secretory cell differentiation within the zebrafish intestinal epithelium resulting in a loss of distal intestinal motility. *Developmental Biology* **376**, 171–186.

[55] AS Rolig, R Parthasarathy, AR Burns, BJ Bohannan, and K Guillemin. (2015) Individual Members of the Microbiota Disproportionately Modulate Host Innate Immune Responses. *Cell Host & Microbe* **18**, 613–620.

[56] R Rusconi, JS Guasto, and R Stocker. (2014) Bacterial transport suppressed by fluid shear. *Nature Physics* **10**, 212–217.

[57] M Saadatmand, T Ishikawa, N Matsuki, M Jafar Abdekhodaie, Y Imai, H Ueno, and T Yamaguchi. (2011) Fluid particle diffusion through high-hematocrit blood flow within a capillary tube. *Journal of Biomechanics* **44**, 170–175.

[58] AM van der Sar, RJP Musters, FJM van Eeden, BJ Appelmelk, CMJE Vandenbroucke-Grauls, and W Bitter. (2003) Zebrafish embryos as a model host for the real time analysis of *Salmonella typhimurium* infections. *Cellular Microbiology* **5**, 601–611.

[59] I Sekirov, SL Russell, LCM Antunes, and BB Finlay. (2010) Gut Microbiota in Health and Disease. *Physiological Reviews* **90**, 859–904.

[60] P Servais, G Billen, and JV Rego. (1985) Rate of bacterial mortality in aquatic environments. *Applied and environmental microbiology* **49**, 1448–1454.

[61] JT Shin and MC Fishman. (2002) FROM ZEBRAFISH TO HUMAN: Modular Medical Models. *Annual Review of Genomics and Human Genetics* **3**, 311–340.

[62] ICH Smith. (1972) Energetics of activation in frog and toad muscle. *The Journal of physiology* **220**, 583.

[63] R Spence, G Gerlach, C Lawrence, and C Smith. (2007) The behaviour and ecology of the zebrafish, Danio rerio. *Biological Reviews* **83**, 13–34.

[64] MJ Tindall, PK Maini, SL Porter, and JP Armitage. (2008) Overview of Mathematical Approaches Used to Model Bacterial Chemotaxis II: Bacterial Populations. *Bulletin of Mathematical Biology* **70**, 1570–1607.

[65] C Tropini, KA Earle, KC Huang, and JL Sonnenburg. (2017) The Gut Microbiome: Connecting Spatial Organization to Function. *Cell Host & Microbe* **21**, 433–442.

[66] S Vaishnava, M Yamamoto, KM Severson, KA Ruhn, X Yu, O Koren, R Ley, EK Wakeland, and LV Hooper. (2011) The Antibacterial Lectin RegIIIg Promotes the Spatial Segregation of Microbiota and Host in the Intestine. **334**, 5.

[67] KN Wallace, S Akhter, EM Smith, K Lorent, and M Pack. (2005) Intestinal growth and differentiation in zebrafish. *Mechanisms of Development* **122**, 157–173.

[68] KN Wallace and M Pack. (2003) Unique and conserved aspects of gut development in zebrafish. *Developmental Biology* **255**, 12–29.

[69] C Westerwalbesloh, A Grünberger, B Stute, S Weber, W Wiechert, D Kohlheyer, and E von Lieres. (2015) Modeling and CFD simulation of nutrient distribution in picoliter bioreactors for bacterial growth studies on single-cell level. *Lab Chip* **15**, 4177–4186.

[70] R White, K Rose, and L Zon. (2013) Zebrafish cancer: the state of the art and the path forward. *Nature Reviews Cancer* **13**, 624–636.

[71] TJ Wiles, M Jemielita, RP Baker, BH Schlomann, SL Logan, J Ganz, E Melancon, JS Eisen, K Guillemin, and R Parthasarathy. (2016) Host Gut Motility Promotes Competitive Exclusion within a Model Intestinal Microbiota. *PLOS Biology* **14**, e1002517.

[72] J Yang, Y Shimogonya, and T Ishikawa. (2017) Mixing and pumping functions of the intestine of zebrafish larvae. *Journal of Theoretical Biology* **419**, 152–158.

[73] LI Zon and RT Peterson. (2005) In vivo drug discovery in the zebrafish. *Nature Reviews Drug Discovery* **4**, 35–44.

Acknowledgements

Completion of my Ph.D. course at the Biological Flow Studies Laboratory of Tohoku University was possible with the support of several people. So I would like to express my sincere gratitude to all of them.

First, I would like to express my special appreciation and thanks to My advisor, Professor Takuji Ishikawa, for his patience, motivation, enthusiasm, and immense knowledge. He was continue to guide and support me during these past three years and let me complete this doctoral dissertation as possible. He always instructed me how to grow as a research scientist and encouraged my research with many warm words. He provided me many valuable opportunities to express myself and study at international conference around the world. I thank my advisor whole heartedly, not only for his tremendous academic support, but also for giving me so many wonderful opportunities. I can never thank him enough. It has been surely a great experience for me to have him as my Ph.D. advisor, just as my thought when I meet him first time. 石川先生、誠にありがとうございました。

I would also like to thank Associate Professor Shimogonya, Yuji. He was very kind to me like a tutor during the first two years of my Ph.D. course. He not only supported and advised me on my research work, but also help me a lot to adapt the life in Japan. During that two years, our desks were against each other. When I encountered problem or trouble, I always received friendly help from him as soon as possible. Thank you very much, *Shimogonya sensei*.

Professor Kouhei Fukushima and Professor Makoto Ohta, thanks a lot for their critical comments and valuable advices about this thesis.

Associate Professor Kenji Kikuchi, thanks a lot for his the viewpoint of researchers in the experiment and provided me the ”recommendation letter” for the

application of JSPS. Assistant Professor Toshihiro Omori, thanks a lot for his tender help, advise and discussion, especially when I moved to his room in the last year of my Ph.D. course. Thanks a lot Associate Professor Keiko Numayama-Tsuruta, I received many advices from her a biological point of view. All the professors in BFSL laboratory, Thank you very much.

Thanks all the students of BFSL laboratory, for their kind help and providing me cheerful days. Owing to all the members of BFSL, I have had wonderful time during these three years.

Secretaries of BFSL laboratory, especially *Chida san*, thanks a lot for their outstanding assistance and encouragement during my laboratory life.

A special thanks to my family. Words cannot express how grateful I am to my mother-in-law, father-in-law, my mother, and father, my son, my wife for all of the sacrifices that they have made on my behalf. Especially, I really really want to thank my wife. As an international student, without her support, understanding, encouragement and great sacrifice, I could not have done this work.

Jinyou Yang

January 2019.

Research Accomplishments

Journal papers related to this thesis

[1] **J Yang**, Y Shimogonya, and T Ishikawa. (2018) What causes the spatial heterogeneity of bacterial flora in the intestine of zebrafish larvae? *Journal of Theoretical Biology* **446**, 101–109.

[2] **J Yang**, Y Shimogonya, and T Ishikawa. (2017) Mixing and pumping functions of the intestine of zebrafish larvae. *Journal of Theoretical Biology* **419**, 152–158.

Other journal papers

[1] **J Yang**, Y Shimogonya, and T Ishikawa. (2019) Bacterial detachment from a wall with a bump line. *Physical Review E* **99**, 023104.

Following papers were written in Chinese.

[2] **J Yang**, Y Wang, J Liu, H Yu, and Y Hong. (2015) Observation of hemodynamics in human descending aorta after V-shaped stent implantation. *Shandong Medical Journal* **7**, 11–14.

[3] J Liu, **J Yang**, and Y Hong. (2015) Numerical Simulation Analysis of Hemodynamics in Human Vertebral Artery under the Normal Position. Chinese *Journal Of Medical Physics* **32**, 110–114.

[4] **J Yang**, H Yu, J Liu, and Y Hong. (2014) Layered abdominal aortic aneurysm model based on fluid-structure interaction. *Biomedical Engineering and Clinical Medicine* **18**, 310–314.

[5] **J Yang**, H Yu, J Liu, and Y Hong. (2014) Numerical Simulation in two- phase Blood Flow in Stenosis of Vertebral Artery. *Progress in Modern Biomedicinee* **14**, 3410–3413.

[6] **J Yang**, J Liu, H Yang, H Yu, and Y Hong. (2014) A study on iliac aortic with thrombosis based on Fluid-Solid Interaction numerical simulation. *Chinese Journal Of Medical Physics* **31**, 4941–4947.

[7] **J Yang**, H Yang, J Liu, H Yu, and Y Hong. (2013) Blood flow in hu- man aortic arch with fluid-structure interaction coupled computational fluid dynamic simulation. *Biomedical Engineering and Clinical Medicine* **17**, 1–5.

[8] Y Xu, **J Yang**, H Yu, J Liu, and Y Hong. (2012) Analysis blood flow in bifurcation of abdominal aorta based on computational fluid dynamics method. *China Journal of Modern Medicine* **22**, 36–40.

[9] **J Yang**, J Liu, H Yu, J Guo, and Y Hong. (2012) Comparison of hemodynamics in iliac aortic with thrombosis and normal iliac aortic based on numerical simulation. *Biomedical Engineering and Clinical Medicine* **16**, 1–6.

[10] Y Xu, **J Yang**, Z Liu, and Y Hong. (2011) Analysis the no heating reasons of P - 97 Micro electrode drawing instrument. *Chinese Medical Equipment Journal* **32**, 99–100.

[11] **J Yang**, Y Xu, H Yu, J Liu, J Shan, J Guo, and Y Hong. (2011) Numerical Simulation the Non-Newtonian Blood Blow in Human Aortic Arch. *Chinese Journal Of Medical Physics* **28**, 2422–2425.

[12] **J Yang**, H Yu, J Liu, J Shan, J Guo, and Y Hong. (2010) Comparison of blood flow dynamics in thoracic aortic dissection and normal aortic based on CT images. *Biomedical Engineering and Clinical Medicine* **14**, 390–393.

[13] **J Yang**, H Yu, J Shan, J Guo, and Y Hong. (2010) Comparative Analysis Different Individuals of the Aortic Arch of Blood Flow Simulation Based on Computational Fluid Dynamics Methods. *Chinese Journal Of Medical Physics* **27**, 2059–2062.

[14] R Xiang and **J Yang**. (2008) External Circuit Effecting on the Stability of Discharge Current of Low-pressure Air Light. *Science Technology and Engineering* **8**, 172–173.

[15] **J Yang** and R Xiang. (2007) Teaching On The Design of Medical Physics Experiment. *Journal of Liaoning University of Traditional Chinese Medicine* **9**, 204–205.

International Conferences

[1] **J Yang**, Y Shimogonya, and T Ishikawa. (2018) Spatial heterogeneity of bacterial flora in the intestine of zebrafish larvae. *8TH World Congress of Biomechanics.*

[2] **J Yang**, Y Shimogonya, and T Ishikawa. (2017) Transport phenomena in the intestine of zebrafish larvae. *5TH SWITZERLAND-JAPAN WORKSHOP ON BIOMECHANICS SJB.*

[3] **J Yang**, Y Shimogonya, and T Ishikawa. (2016) Numerical study on mixing and pumping functions generated by peristalsis in a zebrafish intestine. *The 16th International Conference on Biomedical Engineering.*

Domestic Conferences

[1] 楊金有, 下權谷祐児, 石川拓司, ゼブラフィッシュの腸内フローラシミュレーション, 日本流体力学会年会 2018 年度年次大会, 講演論文集 No.030, 大阪 (2018 年 9 月).

[2] 楊金有, 下權谷祐児, 石川拓司, ゼブラフィッシュ稚魚の腸内輸送現象のシミュレーション, 日本流体力学会年会 2017 年度年次大会, 講演論文集 No.007, 東京 (2017 年 9 月).

[3] 楊金有, 下權谷祐児, 石川拓司, ゼブラフィッシュ稚魚の腸内流れのシミュレーション, 日本機械学会第 29 回バイオエンジニアリング講演会, 講演論文集 1G45, 名古屋 (2017 年 1 月).

Other Conferences

[1] **J Yang** and Y Hong. (2011) Numerical Simulations of the Non-Newtonian Blood Blow in Human Thoracic Aortic Dissection Based on CT images. *The 5th International Conference on Bioinformatics and Biomedical Engineering.*

[2] **J Yang** and Y Hong. (2011) Numerical Simulations of the Non-Newtonian Blood Blow in Human Abdominal artery Based on Reverse Engineering. *SREE Workshop on Medical Materials and Engineering.*

[3] **J Yang** and Y Hong. (2010) Application of computational fluid dynamics method of simulation analysis of thoracic aortic blood flow. *Great Wall 2010 International Congress on Medical Physics.*

Awards

2017 TRAVEL AWARD
5th Switzerland-Japan workshop on biomechanics

2018 東北大学藤野先生記念奨励賞